Journal of Molecular Liquids 336 (2021) 116315

Contents lists available at ScienceDirect

Journal of Molecular Liquids

journal homepage: www.elsevier.com/locate/molliq

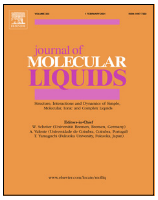

Integrated modeling, surface, electrochemical, and biocidal investigations of novel benzothiazoles as corrosion inhibitors for shale formation well stimulation

Ahmed A. Farag [a,d,*], A.M. Eid [b,*], M.M. Shaban [a,*], Eslam A. Mohamed [a,d], Gunasunderi Raju [c]

[a] Egyptian Petroleum Research Institute (EPRI), Nasr City, 11727 Cairo, Egypt
[b] Mansoura Petroleum Company, 11728 Cairo, Egypt
[c] Chemistry Section, School of Distance Education, Universiti Sains Malaysia, Penang, Malaysia
[d] Faculty of Science, Mansoura University, Egypt

ARTICLE INFO

Article history:
Received 10 October 2020
Revised 16 April 2021
Accepted 25 April 2021
Available online 28 April 2021

Keywords:
Well stimulation
Biocidal activity
SEM
EDX
DFT
Monte Carlo simulation

ABSTRACT

Three novel benzothiazole-based structures (BTPM series) were investigated for their anticorrosion and biocidal effectson N80 carbon steel alloys. BTPM series molecules were tested against the acidization stimulation process of shale formations oil wells, as well as their antibacterial performance as biocidal agents against water fracturing well stimulation. The anticorrosion evaluation used gravimetric and electrochemical techniques in 1 mol·dm^{-3} (9.86 wt%) HCl solution. Benzothiazole derivatives, namely, (E)-N-(benzo[d]thiazol-2-yl)-1-phenylmethanimine (H-BTPM), (E)-N-(6-methylbenzo[d]thiazol-2-yl)-1-phenyl methanimine (Me-BTPM), and (E)-2-(benzylideneamino) benzo[d]thiazole-6-thiol (SH-BTPM), were studied using chemical and electrochemical techniques. Experimental data showed that the inhibition efficiency of H-BTPM, Me-BTPM, and SH-BTPM for 1×10^{-2} mol·dm^{-3} reached 78%, 82%, and 90%, respectively. The tested compounds were found to comply with Langmuir adsorption isotherm. Quantum chemical calculations were performed to provide a rationalization for the obtained experimental data. Results of the microbial assay revealed the excellent bioactivity of the BTPM series against selected isolated bacterial strains known for their aerobic corrosion effect, emphasizing the role of these novel structures as potential biocides.

1. Introduction

Most industrial processes use acidic solutions during routine operations. These processes (e.g., acidization in oil and gas wells) are performed to enhance the production of mature oil wells [1]. Unfortunately, these acidic solutions have an aggressive corrosive effect on metallic structures [2]. Organic corrosion inhibitor additives are commonly used to reduce such acid corrosion attacks on metallic structures [3–7]. Most of these organic compounds are structurally designed to include certain moieties, such as heterocyclic rings, polar groups, conjugated double bonds, or heteroatoms (N, O, S, and P), which support their application as potent corrosion inhibitors [8–14]. These moieties can easily be adsorbed by the metallic substrate by either physical adsorption or by chemical adsorption on the metal substrate [15–19]. Among these organic corrosion inhibitors, benzothiazole and its derivatives have proven effective in protecting steel surfaces against aggressive acidic solutions [20–29]. Benzothiazole compounds can be structurally defined as cyclic molecules that possess active centers that can adhere to metal surfaces, in particular, the conjugated double bonds via the fused benzene ring and the imine functional group (—C=N—), in addition to the sulfur and nitrogen heteroatoms. Heterocyclic compounds are considered one of the most utilized active ingredients in approximately 70% of antibacterial drugs. Benzothiazole-based compounds are used amid these heterocyclic active antimicrobial agents due to their capability to disrupt the integral membrane protein of the bacterial cell at the membrane/water interface [30–34]. Computational quantum mechanics (QM) can be considered a powerful technique to analyze the corrosion inhibition mechanism of organic compounds [35–37]. This can be assessed by its ability to provide a comprehensive detail for the electronic configuration of a defined molecular structure, as well as intermolecular interactions and reaction mechanisms by utilizing its renowned density functional theory (DFT) technique [38,39]. At present, the DFT technique has been extensively used to deduce

---

* Corresponding authors.
E-mail addresses: ahmedafm@yahoo.com (A.A. Farag), aeid@mansourapeteg.com (A.M. Eid), mahmoud_shaban26@yahoo.com (M.M. Shaban).

https://doi.org/10.1016/j.molliq.2021.116315
0167-7322/

many electronic properties, by which the corrosion inhibition performance can be evaluated [39–41]. Together with other computational methods, such as Monte Carlo (MC) simulations, it can be used as an effective and reliable approach to promote the construction of new molecular structures with customized properties. This combination of MC and DFT is already being adopted as an essential part of holistic material design systems, such as integrated computational material engineering (ICME) [42–47]. This work aims to provide new synthesized, easy, eco-friendly, multifunctional benzothiazole inhibitors for metallic corrosion and bacterial growth inhibition. The corrosion inhibition activity is investigated via a novel proposed design of three derivatives, namely, (E)-N-(benzo[d]thiazol-2-yl)-1-phenylmethanimine (H-BTPM), (E)-N-(6-methylbenzo[d]thiazol-2-yl)-1-phenylmethanimine (Me-BTPM), and (E)-2-(benzylideneamino) benzo[d]thiazole-6-thiol (SH-BTPM) for N80 carbon steel protection against 1 mol·dm^{-3}HCl solution. The implemented concentration of 1 mol·dm^{-3} HCl (3 wt%) solution is used for the acidization materix for carbonate-rich shale formation oil wells [48–50]. Accordingly, BTPM series molecules was tested against such acidization process, as well as aganist microbial contamination that may be introduced to the wellbore due to the hydraulic cracking job [51–54]. Corrosion inhibition evaluations are conducted by chemical weight loss, electrochemical impedance spectroscopy (EIS), and potentiodynamic polarization (PDP) techniques. A surface imaging study of the exposed steel specimen is analyzed using scanning electron microscopy (SEM) and energy dispersive analysis of X-rays (EDX). The biocidal activity of the designed molecules is tested against several active bacterial strains, in particular, Staphylococcus aureus (DSMZ 3463), Bacillus subtilis (ATCC 6633), Pseudomonas aeruginosa (ATCC 9027), and Escherichia coli (ATCC 8739), which are known for their induced corrosion action [55–57]. Lastly, a computational study is conducted to offer theoretical reasoning for the accountability of the synthesized structures to the resulting experimental corrosion inhibition efficiency.

2. Experimental

2.1. Synthesis of benzothiazole derivatives

The studied benzothiazole compounds (Fig. 1) were first synthesized as a Schiff base ligand ordinarily through a condensation reaction (1:1 mol ratio) of benzaldehyde with benzo[d]thiazol-2-amine, 6-methylbenzo[d]thiazol-2-amine, and 2-aminobenzo[d]thiazole-6-thiol to produce H-BTPM, Me-BTPM, and SH-BTPM, respectively; the three products are denoted as the BTPM series. The reactions were induced by adding a solution of benzaldehyde in methyl alcohol (2 ml) separately to each amine predissolved in methyl alcohol (5 ml). Then, the mixture was stirred for 10 h. Lastly, the produced yield was filtered and washed by methyl alcohol.

2.2. Characterization of synthesized benzothiazole derivatives

Fig. 2(a) shows the FTIR spectra of the produced SH-BTPM as a representative example. A weak band at 2600–2550 cm^{-1} was present due to the existence of the SH group, whereas the band at 1200–1050 cm^{-1} corresponded to the —C—S—bond. S—CH$_2$ was at 2880–2845 cm^{-1}, and the characteristic peak of the imine group —(CH=N—) was at 1670–1600 cm^{-1}. Fig. 2(b) shows the ^{1}H NMR spectrum chart (δ ppm) of synthesized SH-BTPM, which comprises signals at δ = 3.4 related to the proton of the thiol group (—SH), δ = 7.5 due to five protons of the two benzene rings that were away from the thiazole ring, δ = 7.8 related to three protons of the two benzene rings that were near to the thiazole ring, and δ = 9 corresponding to the proton of the imine group (—CH=N—).

2.3. Antimicrobial activity

In the present study, the antibacterial action of the synthesized benzothiazole derivatives was estimated using the modified agar disk diffusion method. The standard bacterial strains Staphylococcus aureus (DSMZ 3463), Bacillus subtilis (ATCC 6633), Pseudomonas aeruginosa (ATCC 9027), and Escherichia coli (ATCC 8739) were stacked on the surfaces of nutrient-agar plates. Furthermore, 0.1 ml of the synthesized benzothiazole products was added to a sterile 10 mm borer's well and kept overnight at 37 °C. Then, antibacterial susceptibility was estimated by measuring the clearing zones (mm). This experiment was performed twice. In parallel, the negative control was sterile water, and the positive controls were standard antibiotics. Furthermore, the % activity index was computed by the following equation [58]:

$$\%\ Activity\ index = \frac{inhibition\ zone\ of\ the\ test\ compounds}{inhibition\ zone\ of\ the\ standard\ drug} \times 100 \qquad (1)$$

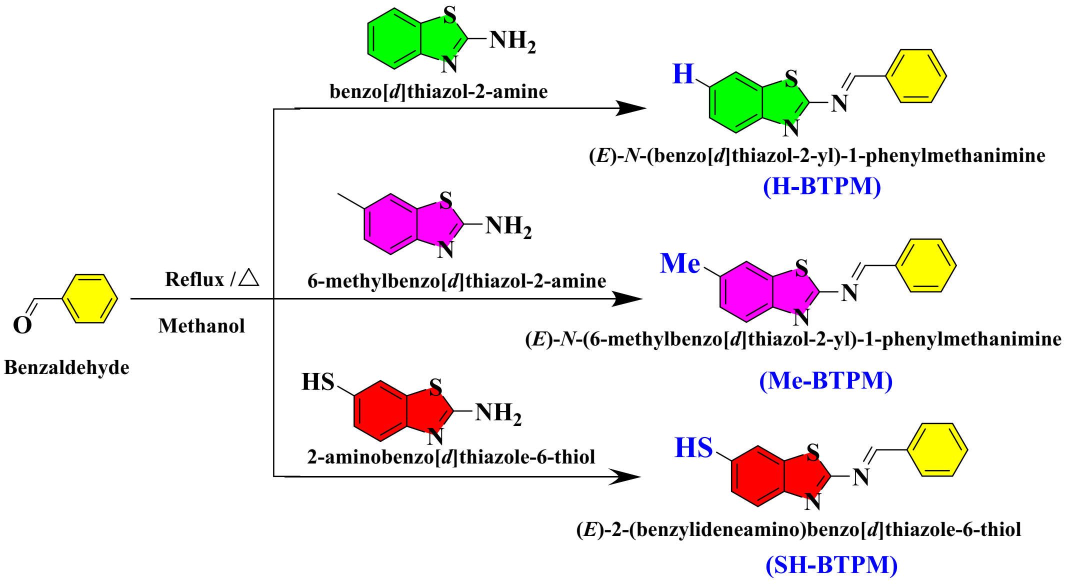

Fig. 1. Synthesis scheme of the three benzothiazole derivatives.

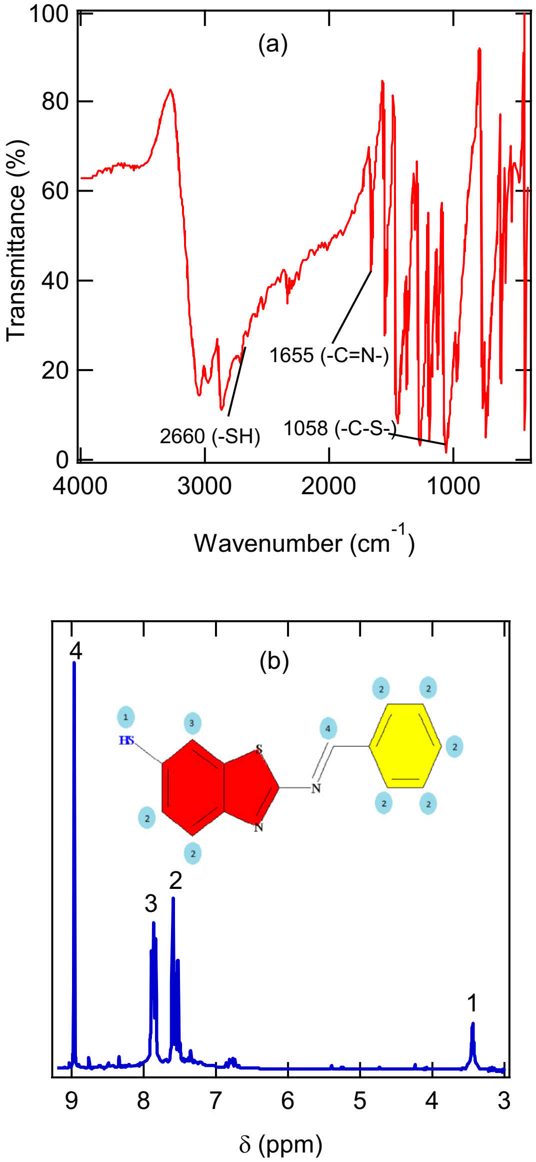

Fig.2. (a) FTIR and (b) ^{1}H NMR of SH-BTPM.

Minimal inhibitory concentration (MIC) is considered the lowest required concentration of a biocidal agent for inhibiting all the progression of the visible microbial growth during a bioassay test. Meanwhile, minimal biocidal concentration (MBC) is regarded as the lowest required concentration of a biocidal agent for exterminating 99% of the proliferated germs. The MIC and MBC of the prepared benzothiazole derivatives were evaluated by applying the broth microdilution method using a 96-sample microwell plate method, as previously stated in the Amsterdam protocol with further considerations. The inoculation preparations were propagated by the cultivation of the purchased bacterial strains in Difco$^{\mathrm{TM}}$ Mueller–Hinton broth purchased from BD Biosciences, USA. The experimental inocula were prepared as previously described by Miller *et al.*, 2005 [59].

Microwell plates from Nunclon$^{\mathrm{TM}}$, Germany (F, PS, non-TC-treated) were applied to determine the MICs. The MICs of the synthesized benzothiazole derivatives were estimated using the two-fold microdilution technique. In the beginning, the benzothiazole derivatives (100 μl) were dispensed onto the microwell plates for further inoculation with the prepared microbial inoculum suspension (100 μl). Only one column was marked as the positive control for the evaluated benzothiazole derivatives (only media, inoculum, without derivatives), whereas another column was marked as the negative control (only media, no inoculum, no derivatives). The microwell plates were incubated under aerobic conditions at 37 °C for a 20–22 h duration. The MBC values of the benzothiazole derivatives were estimated via the removal of media that display no visual microbial development from the wells, followed by their subculturing onto agar plates. These agar plates were subsequently incubated until the microbial development becomes visible in the control plates at 37 °C for a 20–22 h incubation period [60].

2.4. Preparation of samples and solutions

N80 carbon steel coupons were precisely cut from a well tubing line with dimensions of 73 mm × 22 mm × 3 mm to be used in gravimetric weight loss analysis. Electrochemical measurements of corrosion were conducted on N80 carbon steel specimens with the following elemental analysis (wt%): 0.47% C, 0.24% Si, 0.16%, Cr, 0.08% Ni, 0.09% Cu, and the rest is Fe. The steel sample was shaped into a cylindrical working electrode (WE), which was covered with Teflon (except for a 1 cm^2 area that faces the corrosive electrolyte). The WE specimen was abraded by emery papers with various grades starting from 800 grit to 2000 grit. Then, it was rinsed with distilled water, washed with acetone/ethanol mixture to remove any accumulated grease, and then dried. The corrosive electrolyte of 1 mol·dm^{-3} was formed by dilution of analytical grade HCl with a concentration of 37% using bidistilled water. Various inhibitor concentrations (1×10^{-5}–1×10^{-2} mol dm^{-3}) were prepared. All tests were conducted in triplicate to obtain the appropriate one.

2.5. Gravimetric weight loss measurements

Gravimetric measurements were conducted in accordance with ISO 9226:2012-Eq. (1) standard methods [61]. N80 carbon steel coupons were precisely weighed and then dipped in a beaker containing 200 ml of 1 mol·dm^{-3} HCl in the presence and absence of various inhibitor concentrations at a temperature of 30 °C . After 24 h, the coupons were removed from the solution, carefully washed with distilled water, ultrasonically cleaned in acetone/ethanol mixture, dried, and finally precisely weighed again. All tests were conducted in triplicate to obtain the average and ensure data repeatability. To calculate the rate of corrosion (ν, mg cm^{-2}-h^{-1}) and the efficiency (η_w), the following equations were used [62]:

$$\nu = \frac{\Delta W}{St} \tag{2}$$

$$\eta_w = \left[\frac{\nu_{\circ} - \nu}{\nu_{\circ}}\right] \times 100 \tag{3}$$

where ΔW is the average loss of weight; *S* is the exposed area of the coupon (cm^2); *t* is the time of immersion (h); ν_o and ν are the corrosion rate values of uninhibited aggressive (blank) and inhibited electrolytes, respectively.

2.6. Electrochemical measurements

The electrochemical measurements were performed using a Volta-Lab model PGZ402 potentiostat with a Volta-Master 4 software package V7.8. The potentiostat was connected to a conventional cell with a three-electrode arrangement in the following manner: N80 carbon steel specimen as the WE, platinum rode as the counter/auxiliary electrode, and saturated calomel electrode (SCE) as the reference electrode. The measurements started with the immersion of WE in the electrolyte for 1 h to establish the open circuit potential (OCP) steady state. The EIS measurements were conducted within the frequency range of 100 kHz to 0.03 Hz at OCP with a 10 mV amplitude using an AC signal. The PDP measurements were performed in a potential range of −900–200 mV (vs. SCE) with a 1 mV s^{-1} scan rate [63,64]. All tests were conducted in triplicate to achieve improved data repeatability.

2.7. Quantum chemical studies

2.7.1. QM modeling

The computational quantum parameters were calculated using the Spartan v.14 software package by Wavefunction, Inc. The geometrical structure was optimized using the semiempirical method, parametric method 3. Afterward, DFT molecular orbital calculations were used to estimate the required quantum chemical descriptors accurately [65]. DFT measurements were conducted via a 6–31G* basis set using a Beck-3 parameter Lee Yang Parr (B3LYP) hybrid Hartree-Fock/DFT function and a conductor-like polarizable continuum model for solvation energy calculations [66,67]. The calculated descriptors involved the following: frontier molecular orbital energies (E_{HOMO} and E_{IUMO}), absolute electronegativity(χ), global electrophilicity index (ω), total energy (E_T), and dipole moment (μ).

2.7.2. MC simulations

To imitate the adsorption process of the molecules under study on a certain crystalline surface, the MC simulation algorithm was utilized for an improved understanding of the corrosion inhibition mechanism. Using such technique, the binding energy between the corrosion inhibitor and a selected substrate of steel crystal, which represents the exposed surface to corrosive attack, can be measured using the Material Studio 17 Suite package from BIOVIA. First, an iron crystal was cleaved with a selected (1 1 0) index plan, which represents the main growth plan for an iron crystal for its bulk-terminated arrangement with minimum relaxation effects and with no surface reconstructions [68]. This plane was further expanded to a three-dimensional supercell of 43 Å × 43 Å × 27 Å proportions using periodic boundary conditions to confirm homogeneous loading for all the added particles on the substrate surface [69]. The embedded adsorption locator module was utilized by employing simulated annealing algorithm and COMPASS forcefield. Water molecules and chloride ions were inserted into the module that mimics the corrosive medium that was loaded to the steel surface.

3. Results and discussion

3.1. Gravimetric measurements

Fig. 3(a) depicts the curves of the concentrations of the investigated BTPM series inhibitors vs. the corrosion rates (ν) of N80 carbon steel immersed in the 1 mol·dm^{-3} HCl at room temperature for 24 h. With the increase in inhibitor concentration, the corrosion rate of the N80 carbon steel in the HCl corrosive medium showed a downward trend. This result demonstrates the effective shielding action of the BTPM series against the corrosive attacks of the1 mol·dm^{-3} HCl solution toward the N80 carbon steel surface. The listed corrosion parameters in Table 1 revealed the decline in the corrosion rate values and the consequent rise in the corresponding corrosion inhibition efficiencies after the addition of BTPM series compounds.

The order of inhibitive action of the three BTPM series compounds was as follows: SH-BTPM > Me-BTPM > H-BTPM. This order suggested that the thiol group (—SH) attached to SH-BTPM confirming their added value as a better active center for adsorption on the N80 carbon steel substrate than the methyl group and hydrogen atom in Me-BTPM and H-BTPM, respectively. In addition, when the concentration of SH-BTPM reached 1 × 10^{-2} mol·dm^{-3}, the corrosion inhibition efficiency reached up to 90%. Therefore, the BTPM series can show superior anticorrosion nature [70].

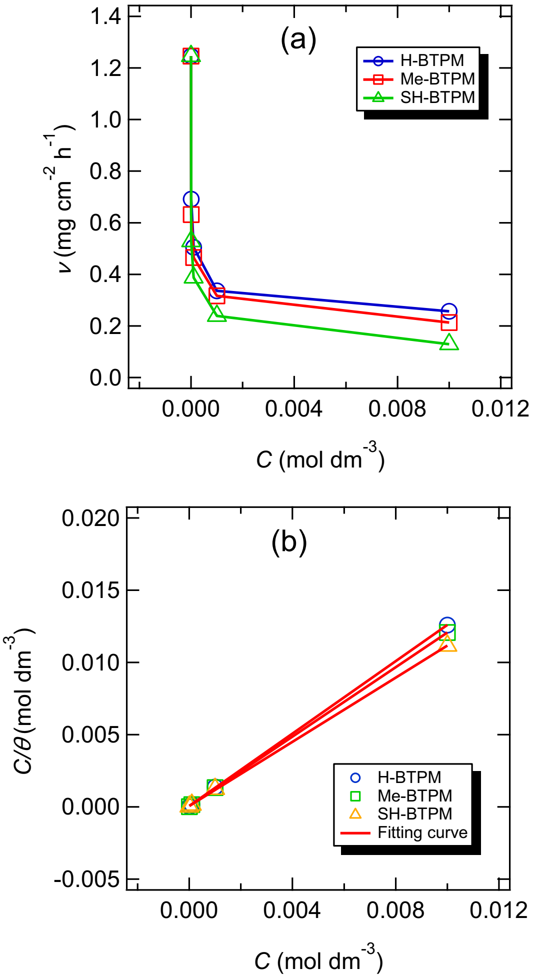

Fig. 3. (a) Variation of the corrosion rate with the inhibitors concentrations, and (b) Langmuir isotherm curves for the inhibitors adsorbed at carbon steel in 1 mol dm^{-3}HCl after 24 h immersion at room temperature.

3.2. PDP test

Fig. 4 portrays the PDP curves of immersed N80 carbon steel samples in the 1 mol·dm^{-3} HCl with and without various concentrations of the three BTPM series inhibitors at room temperature. With the increase in inhibitor concentration, the generated corrosion current density (i_{corr}) for the N80 carbon steel specimen in the hydrochloric acid corrosive medium clearly shows a descending trend. This result confirms the ability of the BTPM series inhibitors to retard the corrosion rate provoked by the acidic solution. An inspection of the PDP plots showed that the anodic and cathodic lines of the curve tended to decline, indicating that the adsorption of BTPM molecules on the carbon steel surface suppressed cathodic hydrogen evolution and anodic dissolution of iron ions. In addition, the polarization curves of the anodic and cathodic branches for the three BTPM inhibitors showed a parallel trend, indicating that that the adsorption of these inhibitors onto the steel surface never changes the corrosion process mechanism. The inhibition efficiency (η_p) can be calculated by the following equation [71]:

Table 1
Weight loss results for carbon steel specimen in 1 M HCl solution after 24 h immersion in the absence and presence of different inhibitors concentrations at 25 °C.

Inhibitor	Conc. (PPM)	CR (mg cm^{-2} h^{-1})	θ	η
Blank	0	1.2463	–	–
H-BTPM	10	0.6918	0.47	47
	20	0.5046	0.56	56
	30	0.3363	0.67	67
	40	0.2563	0.79	79
Me-BTPM	10	0.6319	0.50	50
	20	0.4648	0.60	60
	30	0.3164	0.70	70
	40	0.2131	0.82	82
SH-BTPM	10	0.5284	0.56	56
	20	0.3875	0.66	66
	30	0.2385	0.79	79
	40	0.1295	0.90	90

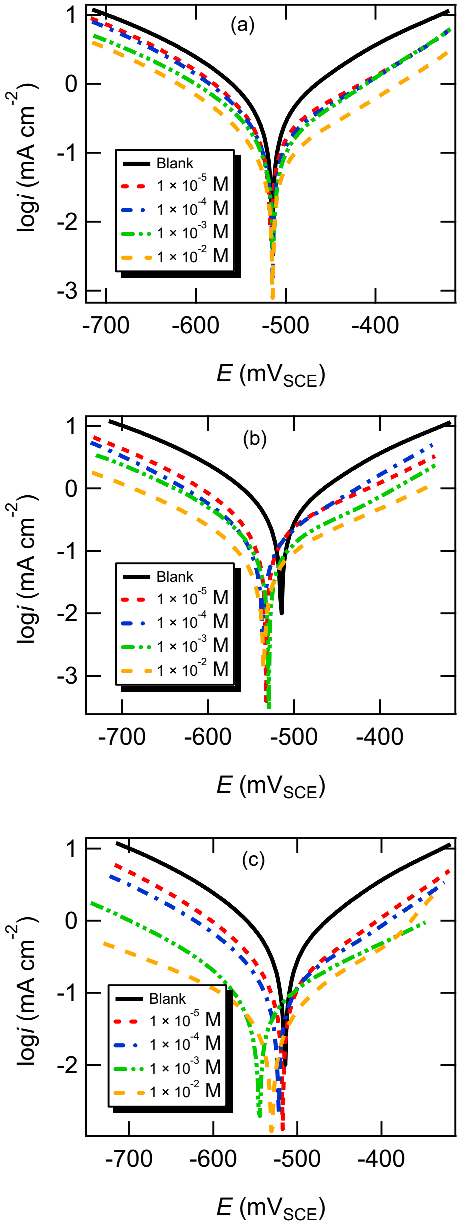

Fig.4. Potentiodynamic polarization curves of carbon steel in 1 mol dm^{-3}HCl with different concentrations of: (a) H-BTPM, (b) Me-BTPM, and (c) SH-BTPM at room temperature.

$$\eta_p = \left[\frac{i^0_{corr} - i_{corr}}{i^0_{corr}}\right] \times 100 \tag{4}$$

where i^0_{corr} and i_{corr} are the corrosion current density without and with BTPM inhibitors, respectively.

Monitoring the corrosion potential (E_{corr}) values listed in Table 2 revealed that after adding the three BTPM inhibitors, the change in such values compared with the blank solution is significantly<85 mV, thus verifying the mixed anodic/cathodic nature of these potential corrosion inhibitors [72–75]. Moroever, when the concentration of the BTPM inhibitors reached 1 × 10^{-2} mol·dm^{-3}, the corrosion inhibition efficiency reached up to 79.3%, 82%, and 90% for H-BTPM, Me-BTPM, and SH-BTPM, respectively. This result proves the ability of the tested benzothiazole derivatives as anticorrosion additives for N80 carbon steel in HCl solution [76].

3.3. EIS test

EIS is a widely utilized tool in the research on corrosion protection of metals. It is an appropriate method for investigating the corrosion process at the metal/electrolyte interface [77]. Fig. 5 outlines the Nyquist and Bode plots of carbon steel in 1 mol·dm^{-3} HCl in the presence and absence of various concentrations of BTPM series inhibitors at room temperature. It can be assumed that after adding these inhibitors to the corrosive solution, all the capacitive loops showed a squashed and imperfect semicircle with the center below the X-axis. This phenomenon is due to the frequency dispersion caused by the adsorption of BTPM molecules onto the carbon steel surface resulting in electrode surface heterogeneity [78]. As shown in Fig. 5, all capacitive loops shape for the three inhibitors curves showed the same style, only the radius of the developed capacitive loops was increased by raising the BTPM inhibitor concentration. This refers to an elevation in charge transfer resistance without introducing any change to the corrosion reaction mechanism. Moreover, the Bode plots for these three inhibitors (Fig. 5) revealed that the phase angle and the absolute impedance curves turned wider and larger with the increase in the BTPM series concentrations; such changes support the inhibition of the action of the BTPM series molecules against N80 steel corrosion in the aggressive HCl electrolyte [79,80]. The electrochemical impedance parameters were quantitatively analyzed using Zsimpwin V3.06 software to fit the electrical equivalent circuit. The best-fit equivalent circuit diagram is represented in Fig. 6, and the fitted data are listed in Table 3. The equivalent circuit includes solution resistance (R_s), charge transfer resistance (R_{ct}), and the constant phase ele-

Table 2
Electrochemical kinetic parameters extracted from the polarization curves for carbon steel in the absence and presence of different inhibitors concentrations at 25 °C.

Inhibitor	C (PPM)	$-E_{corr}$ (mV$_{SCE}$)	i_{corr} (mA cm^{-2})	β_a (mV dec^{-1})	$-\beta_c$ (mV dec^{-1})	θ	η_P (%)
Blank	0	514	1.2023	210	196	–	–
H-BTPM	10	513	0.6033	219	178	0.498	49.8
	20	515	0.4966	204	173	0.587	58.7
	30	516	0.4115	191	188	0.658	65.8
	40	513	0.2488	108	168	0.793	79.3
Me-BTPM	10	530	0.5467	203	177	0.545	54.5
	20	534	0.3801	199	146	0.684	68.4
	30	531	0.3208	207	166	0.733	73.3
	40	533	0.2166	229	170	0.820	82.0
SH-BTPM	10	510	0.4479	189	169	0.627	62.7
	20	521	0.3374	151	155	0.719	71.9
	30	544	0.2508	270	202	0.791	79.1
	40	528	0.1198	159	230	0.900	90.0

ment (*CPE*). C_{dl} is the double-layer capacitor. The *CPE* impedance (Z_{CPE}) and C_{dl} are calculated by the following formulas [81–83]:

$$Z_{CPE} = \frac{1}{Y_0(j\omega)^n} \quad (5)$$

$$C_{dl} = Y_0(\omega)^{n-1} = Y_0(\omega_{Z_{im-Max}})^{n-1} \quad (6)$$

where j is the imaginary unit, Y_0 represents the value of CPE, ω is the angular frequency, and n represents the deviation index. The inhibition efficiency of the BTPM inhibitors can be obtained by the following formula [84]:

$$\eta_i = \left[\frac{R_{ct} - R_{ct}^0}{R_{ct}}\right] \times 100 \quad (7)$$

where R_{ct} and R_{ct}^0 represent the charge transfer resistances with and without BTPM inhibitor. As shown in Table 3, as the concentration of the BTPM series inhibitors is augmented, the value of the corrosion inhibition efficiency becomes significantly larger, indicating that the formed inhibitor film of BTPM molecules onto the carbon steel surface is more ordered and denser [85–88]. While more water molecules on the carbon steel surface are being replaced by BTPM molecules, the thickness of the electric double-layer capacitor (C_{dl}) decreases significantly owing to the associated decrease in the area of exposed N80 carbon steel surface to the 1 mol·dm^{-3} HCl. This phenomenon can be well illustrated by the Helmholtz model [89]:

$$C_{dl} = \frac{\varepsilon_\circ \varepsilon}{d} A \quad (8)$$

where ε_o is the vacuum dielectric constant, ε is the dielectric constant, A is the surface area of the electrode, and d is the thickness of the double layer at the metal surface. In view of these findings, the adsorption of the BTPM series molecules on N80 carbon steel surface was carried out by dispelling the present molecules of water and then forming a denser and more ordered barrier film. This have elicited their ability to impede the electron transfer and generally mitigate the corrosion process [90,91]. These obtained data are compatible with the gravimetric weight loss and PDP data.

3.4. Adsorption isotherm model study

To achieve an improved understanding of the adsorption mechanism of the BTPM series onto the N80 carbon steel surface, the adsorption isotherm must be investigated via the Langmuir model. Such a model assumes only one inhibitor molecular layer adsorbed on the substrate, whereas these molecules do not have any type of interaction with each other. This isotherm can be represented as follows [92,93]:

$$\frac{c}{\theta} = \frac{1}{K_{ads}} + C \quad (9)$$

where C, θ, and K_{ads} represent the inhibitor concentration, the surface coverage, and the adsorption equilibrium constant, respectively. Fig. 3(b) represents the plotted curves of C/θ vs. C, which gave a straight line, and the extracted parameters are listed in Table 4. The linear correlation coefficient (R^2) recorded a value of 0.9999 for the three inhibitors (H-BTPM, Me-BTPM, and SH-BTPM). Table 4 declares the slope close to unity, indicating that the adsorption of the BTPM series on the carbon steel follows the Langmuir model. The adsorption equilibrium constant (K_{ads}) can be calculated from the interception of the isotherm line with the C/θ axis. The large values of K_{ads} indicate that the BTPM series molecules have a strong adsorption ability on the N80 carbon steel surface and hence improved protection against corrosion. In addition, the values of K_{ads} can be used to calculate the Gibbs standard free energy (ΔG^o_{ads}) as follows [94–96]:

$$\Delta G^\circ_{ads} = -RTln(55.5\ K_{ads}) \quad (10)$$

where R is the gas constant, and T the absolute temperature [97]. The listed values of ΔG°_{ads} in Table 4 are negative, indicating that the adsorption of the BTPM series inhibitors on the N80 carbon steel surface is a spontaneous process. It was previously agreed that the inhibitor molecule is physically adsorbed by electrostatic interaction with the negatively charged metal substrate in the presence of Cl^- ions when the $-\Delta G^\circ_{ads}$ value is in the order of 20 kJ·mol^{-1} or below. Furthermroe, the inhibitor molecule would be chemically adsorbed by coordination bonds between its available lone electron pairs and the empty d-orbital of the Fe metal, if the $-\Delta G^o_{ads}$ value is in the order of 40 kJ·mol^{-1} or above [98]. Inspecting the obtained values of $-\Delta G^o_{ads}$, they were as follows; 34.6, 35.1, and 35.5 kJ/mol for H-BTPM, Me-BTPM, and SH-BTPM, respectively as listed in Table 4. Therefore, $-\Delta G^o_{ads}$ ranges between 20 and 40 kJ·mol^{-1}, indicating that the investigated BTPM molecules were of a mixed physical/chemical adsorption nature [99–102].

3.5. Quantum chemical calculations

3.5.1. Quantum mechanical modeling (QM)

Through DFT calculations, frontier orbital energies E_{HOMO} (highest occupied molecular orbital) and E_{LUMO} (lowest unoccupied molecular orbital) were computed, where the former is regarded as an estimation of the electron-donating ability toward an electron-deficient site, and the latter is considered a measure for the ability to receive electrons from a donor [103]. Accordingly, a molecule with a greater E_{HOMO} has a higher chance to donate electrons to the empty d-orbital of the iron substrate and thus may expedite their potential to be adsorbed on the iron surface and

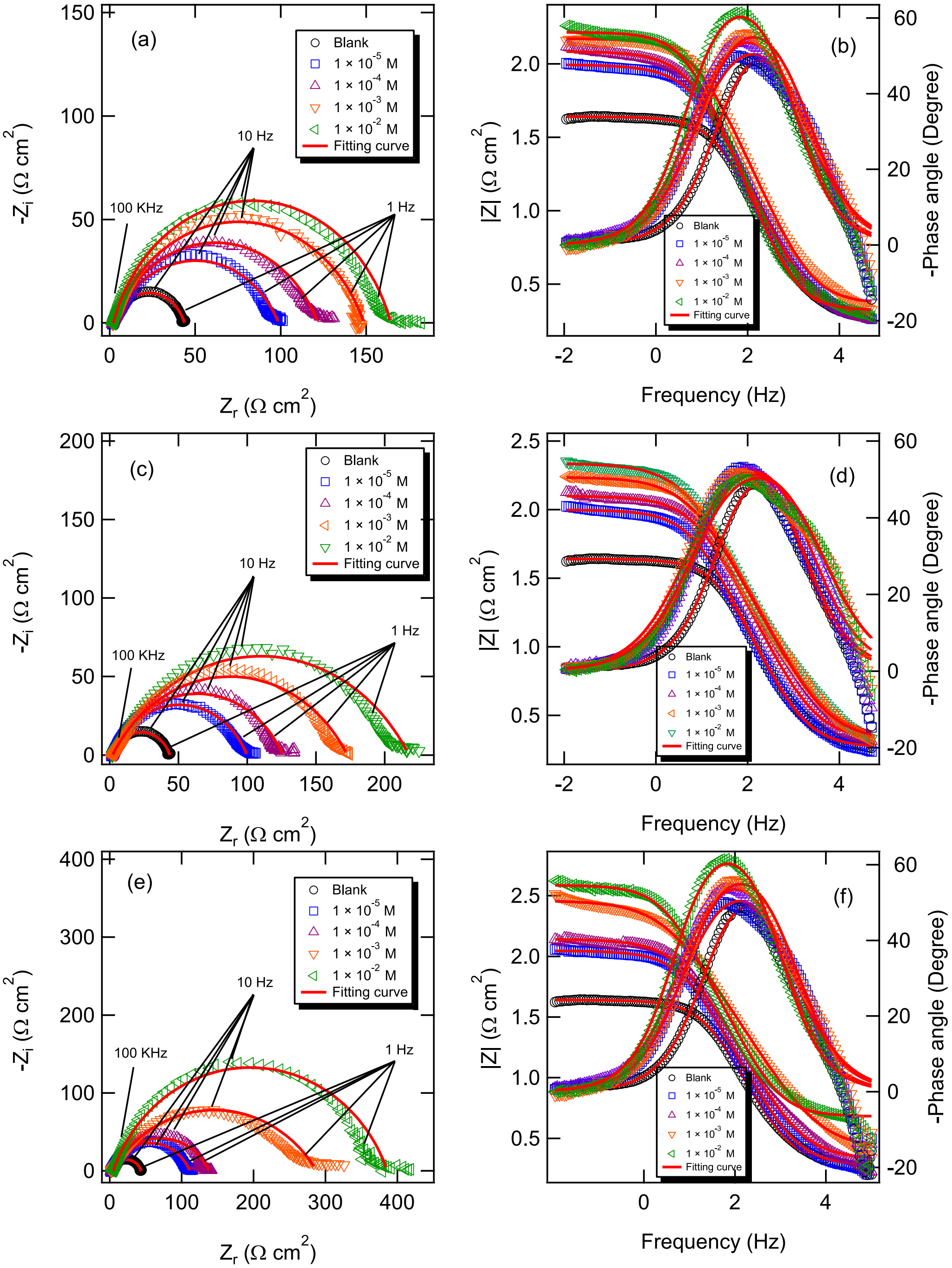

Fig.5. Electrochemical impedance curves of carbon steel in 1 mol dm^{-3}HCl with different concentrations of: (a,b) H-BTPM, (c,d) Me-BTPM, and (e,f) SH-BTPM at room temperature.

enhances the protection against corrosive attacks [104]. Concurrently, as the E_{LUMO} value becomes lower, it can maintain the good adherence property of a molecule by permitting the back-bonding of electrons from the iron surface toward the antibonding π^* orbitals of the inhibitors, which synergistically reinforce their adsorption to the metal surface [105]. On this basis, a narrower energy gap ΔE_{Gap} between a favored high E_{HOMO} level and a low E_{LUMO} level denotes a more firmly adsorbed and simultaneously more efficient corrosion inhibitor [106]. The listed data in Table 5 show lower ΔE_{Gap} values for all BTPM series inhibitors compared with those recently reported in the literature [4,107–110]. SH-BTPM scored the smallest ΔE_{Gap} as compared with Me-BTPM; H-BTPM suitably marks a righteous agreement with the experimental results. E_{HOMO} for the SH-BTPM inhibitor showed the highest value among the three inhibitors, resembling the formerly reported experimental data. For E_{LUMO}, the values for all the BTPM series were almost the same, thus denoting their equivalent ability for back donation due to the extended π-electron delocalization of the conjugated double bond all over the molecule, which effectively lowered the E_{LUMO} level [111]. The listed dipole moment values (μ) showed a rise for SH-BTPM than Me-BTPM and H-BTPM; this rise aligned with its high corrosion inhibition efficiency. In addition, the measured fraction of electron transferred (ΔN) values listed in Table 5 that designates approximations for the number of

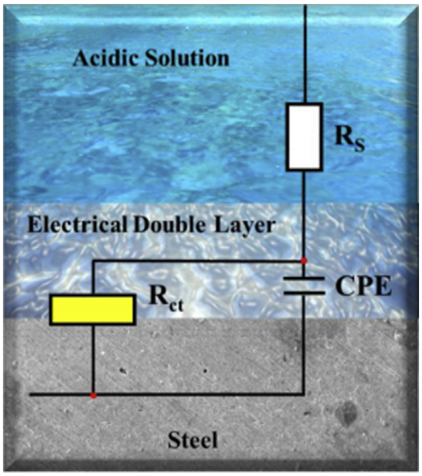

Fig. 6. Equivalent circuit used to model metal/solution interface of carbon steel in 1 mol dm^{-3}HCl in the absence and presence of the benzothiazole derivatives.

donated electrons from the inhibitor molecule to the metallic iron surface was ~ 2.6. Such value was high enough to maintain superb corrosion mitigation properties.

Fig. 7 depicts the surface configuration of higest occupied molecular orbital (HOMO) and Lowest unoccupied molecular orbital (LUMO) for each of the BTPM series molecules. Fig. 7 confirms how HOMO levels in SH-BTPM are majorly localized over the benzothiazole moiety and extended to the thiol group. This would defines a larger electron donation space for SH-BTPM than the same covered area by the methyl group in its counterpart Me-BTPM or hydrogen in H-BTPM. The optimized geometrical structure for all BTPM series (Fig. 7) almost has a planar configuration, which largely assists in covering the entire exposed iron surface in contrast to a bowed configuration. This planar arrangement was attainable due to the designed complete π-bond conjugation over the entire structure [112].

Electrostatic potential mapping (ESP) is considered a useful tool derived from DFT measurements, where it depicts a visual representation for electrophilic and nucleophilic regions according to the color-coded spots on the molecular structure [113]. The color spectrum is scaled from blue to red, where blue regions designate electron-poor moiety and red regions designate electron-rich moiety; the former represents a favored site for electron donation and therefore may serve as an adsorption center [114]. The ESP mapping for the BTPM series molecules (Fig. 8) shows that the red-coded adsorption centers include the N and S heteroatoms in the benzothiazole ring, as well as the amino nitrogen, and extend by using the conjugated aromatic system all over the molecule backbone. By contrast, the ESP mapping for SH-BTPM showed an additional —SH group as an electron-rich site, which imparts additional capacity for the electron donation of the SH-BTPM molecule.

Table 4
Adsorption equilibrium constant (K_{ads}) and standard free energy of adsorption ($\Delta G°_{ads}$) of inhibitors for carbon steel in 1 M HCl solution at 25 °C.

Inhibitor	Slope	The linear correlation coefficient (r^2)	$-\Delta G°_{ads}$ (kJ mol^{-1})
H-BTPM	0.9091	0.9963	28.1
Me-BTPM	0.9161	0.9931	28.5
SH-BTPM	0.9162	0.9886	29.2

The natural bond orbital (NBO) method is viewed as a powerful population analysis for allocating partial electronic charges for all the atoms; thus, it can provide a scale for the nucleophilic behavior all over the molecule [115]. Compared with other population analysis techniques, such as Mulliken charge population analysis, NBO can act as a more improved tool because the former has many disadvantages, including its high dependence on the applied basis set and its frequent assumption of unphysical negative (Pauli violating) values [116–119]. The assigned natural atomic charges for BTPM series molecules are portrayed in Fig. 9. The negatively charged atoms for all the BTPM molecules reveal that the two N atoms demonstrate the most negative behavior, which is extended by the π–bond conjugation to include all the structures that resemble the substantial electron-donating ability. The obtained results listed in Table 5 for the calculated quantum parameters of the investigated BTPM series showed good correlation with the experimental performance, indicating the same trend of corrosion inhibition efficiency (SH-BTPM > Me-BTPM > H-BTPM).

3.5.2. MC simulations

Metropolis MC simulations were conducted using Materials studio software, and its embedded adsorption locator module to validate the electronic interaction process between the loaded inhibitor and the metallic iron substrate. The BTPM series inhibitors were fitted and configured over a (100)-indexed Fe metallic plane. The resulting visualizations are depicted in Fig. 10, and it emphasizes the planar configuration shaped by BTPM series molecules on the Fe metallic surface, thus confirming its ability to cover a larger area and have lower chances for corrosive attacks. The tabulated record of the performed MC simulations in Table 6 describes the calculated descriptors, such as total adsorption energy, rigid adsorption energy, and deformation energy in kcal mol^{-1}. Total energy comprises the energy of the PTMB inhibitor plus the adsorption energy, whereas the latter is defined as the released energy concurrent with the loading and adherence of the inhibitor

Table 3
Impedance electrochemical parameters derived from the Nyquist plots for carbon steel in 1 M HCl solution in the absence and presence of the investigated inhibitors at 25 °C.

Inhibitor	C (PPM)	R_s (Ω cm^2)	Q ($\Omega^{-1}s^n\ cm^{-2}$) × 10^{-4}	n	R_{ct} (Ωcm^2)	C_{dl} (μFcm^{-2})	Error (%)	θ	η_i (%)
Blank	0	1.8	6.56	0.75	40	1553	< 4.07	–	–
H-BTPM	10	1.7	5.77	0.73	96	670	< 4.12	0.58	58
	20	1.7	5.42	0.72	120	542	< 4.07	0.67	67
	30	2.0	4.03	0.71	146	443	< 4.33	0.73	73
	40	1.8	3.29	0.71	163	400	< 5.00	0.75	75
Me-BTPM	10	1.6	4.37	0.73	98	663	< 4.48	0.59	59
	20	1.9	4.32	0.71	123	525	< 4.38	0.67	67
	30	1.9	3.99	0.68	167	302	< 4.24	0.76	76
	40	1.9	3.97	0.67	224	380	< 3.90	0.82	82
SH-BTPM	10	1.7	4.81	0.73	109	593	< 4.36	0.63	63
	20	1.8	4.22	0.69	133	476	< 4.67	0.70	70
	30	2.2	3.18	0.62	284	227	< 4.96	0.86	86
	40	4.4	2.37	0.63	395	170	< 5.03	0.90	90

Table 5
Calculated Different quantum parameters for BTPM series molecules using DFT.

Inhibitor	$E_{HOMO,}$ (eV)	$E_{LUMO,}$ (eV)	ΔE, (eV)	μ (Debye)	Mol. Area, (Å^2)	χ: Absolute electronegativity (eV)	η: Global hardness(eV)	S: Global softness (eV) $^{-1}$	ω: Global electrophilicity index(eV)	ΔE_{bd} : Back donation(eV)	ΔN: Fraction of electron transferred
H-BTPM	−6.02	−2.29	3.73	2.46	257.78	4.155	1.865	0.536	16.099	−0.46625	2.653
Me-BTPM	−5.82	−2.24	3.58	2.38	260.80	4.030	1.790	0.559	14.536	−0.44750	2.658
SH-BTPM	−5.6	−2.52	3.08	4.54	272.25	4.060	1.540	0.649	12.692	−0.38500	2.264

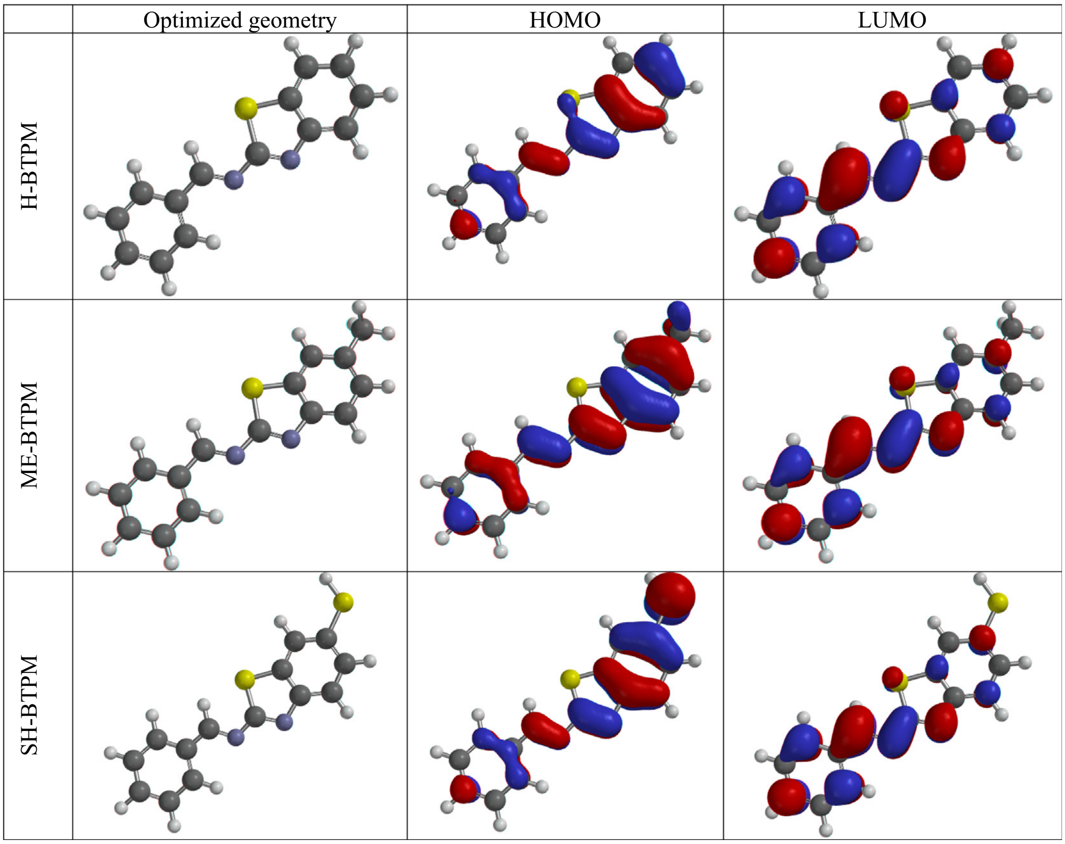

Fig. 7. DFT computational analysis outputs for BTPM series inhibitors.

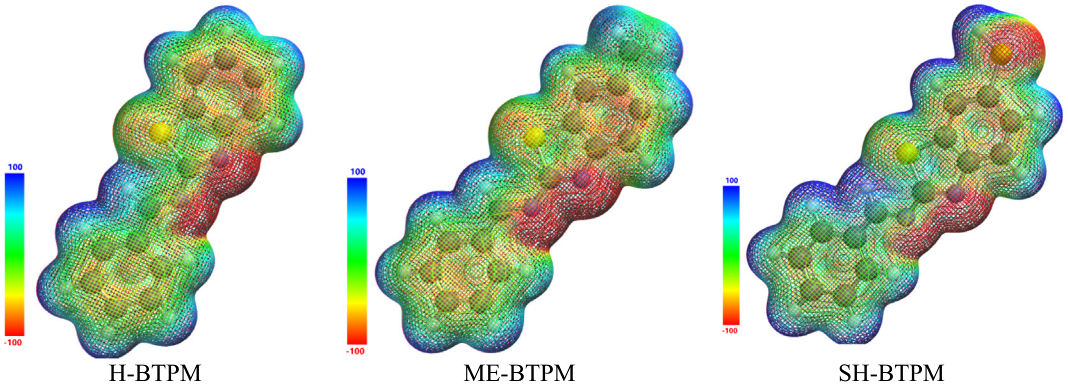

Fig. 8. Electrostatic potential mapping (ESP) for the BTPM series inhibitors.

molecule on the metal surface. The adsorption energy itself is a sum of the rigid adsorption energy, which implies the released energy once the structurally unrelaxed molecules approach the metallic surface, in addition to the deformation energy that expresses the required energy for molecules to endure surface relaxation. The recorded adsorption energy data show that all Al

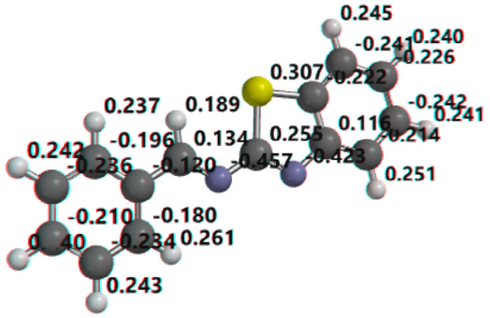

H-BTPM

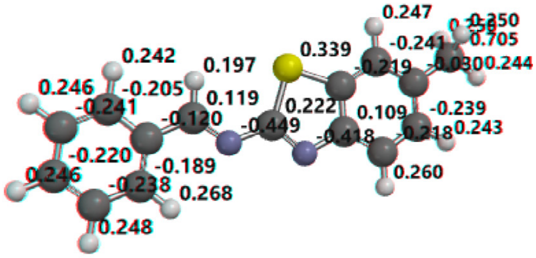

ME-BTPM

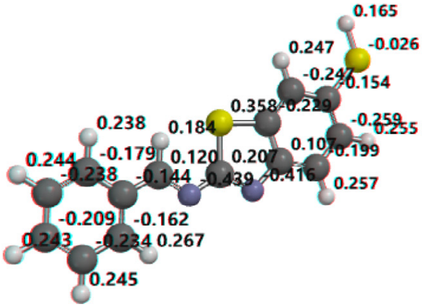

SH-BTPM

Fig. 9. NBO population analysis for the BTPM series.

BTPM series inhibitors scored considerably high negative values (with a slight priority to SH-BTPM), which signify the high tendency of BTPM molecules to be absorbed into the Fe metallic surface [120,121]. The differential adsorption energy (symbolized as dEad/dNi) expresses an indication for the released energy when a particularly sole component is removed [122]. Table 6 reveals that the dE_{ad}/dN_i values for all BTPM series molecules were higher than the dE_{ad}/dN_i value for H_2O molecules, indicating the gradual replacement of water molecules by the more energetically favored BTPM series molecules. Furthermore, the dE_{ad}/dN_i values were − 123.16, −125.60, and − 144.57 for H-BTPM, Me-BTPM, and SH-BTPM, respectively, indicating the dominant adsorption ability for the BTPM series. These findings support the experimental outcomes, primarily in the performance order of BTPM series molecules as corrosion inhibitors (SH-BTPM > ME-BTPM > H-BTPM).

3.6. Antibacterial analysis of the BTPM series

The antibacterial susceptibility of the BTPM series was screened against several bacterial standard strains using the agar well diffusion method. The results are presented in Table 7 and Fig. 11. The obtained data demonstrated higher and broader antibacterial activity in the inhibition clearing zones of 12–27 mm in comparison with standard antibiotics. The biocidal efficacy of these benzothiazole derivatives is powerfully associated with the existence of the heteroatoms (N, O, and S), the benzothiazole ring nucleus, and the azomethine groups (>C═N—in their chemical structures [32].

The high antibacterial activities of these compounds are strongly dependent on the outstanding chemical structures that facilitated their interaction with the microbial cellular membranes. Data in Table 7 and Fig. 11 reveal that among the synthesized molecules, SH-PTBM exhibits the highest antibacterial performance, which can be ascribed to the presence of thiol moiety in its designated structure (*E*)-2-(benzylideneamino)benzo[*d*]thiazole-6-thiol. The presence of heteroatoms (N, O, and S) and azomethine groups in the chemical structures of the BTPM series increases their pathogenic effect against bacteria [123]. The BTPM series can be arranged in accordance with their antibacterial efficacy as follows: SH-BTPM > Me-BTPM > H-BTPM.

Moreover, all these inhibitors show greater antibacterial activity (14–27 mm) for Gram-positive than for Gram-negative bacteria (12–20 mm). This result is probably related to the alteration in the cell wall components between Gram-positive and Gram-negative bacteria. In Gram-positive bacteria, the cell wall embodies only a single peptidoglycan layer, which makes it more sensitive toward many antibacterial agents, whereas for Gram-negative bacteria, the cell wall encompasses additional multilayers of membranes (outer lipid membrane and periplasm) that provide additional resistance against most antibacterial agents [124]. Correspondingly, the mechanism of bacterial cell wall disruption can be related to two main aspects: the number of terminal groups and the biopermeability action. The MIC/MBC values of all BTPM series inhibitors are summarized in Table 8. These inhibitors display lower MICs/MBCs against Gram-positive bacteria (83.3–250.0/104.1–291.6 ppm) than Gram-negative bacteria (125.0–333.3/250.0–500.0 ppm). These results are mainly attributed to the resistivity of the outer cell wall of Gram-negative bacteria deduced from its complex structure of a thick lipid-rich membrane and protein wall, which hinders the entrance of biocidal compounds. However, the inhibition results of the BTPM series are considered to be of a broad-spectrum antibacterial activity in comparison with previously reported studies [125–127]. These effects can be generally related to the formed interaction between the lipoprotein of the bacterial cell wall and heteroatoms or azomethine groups (—CH═N—) of the BTPM series; such interaction leads to a decrease in the osmotic stability of the cell and the leakage of intracellular constituents [128]. Furthermore, the recorded data in Table 8 prove that the lowest MIC/MBC values are attributed to SH-BTPM mostly due to the presence of additional thiol moiety, which identifies the dominant biocidal activity of this compound.

3.7. SEM and EDX surface analysis

SEM surface imaging and EDX surface characterization techniques have been widely implemented in the research fields of metal corrosion to study surface changes before and after different protective measures. Fig. 12 (a–f) show the SEM images and EDX charts of the studied N80 carbon steel surface after 24 h of immersion in 1 mol·dm^{-3} HCl solution without and with 1 × 10^{-2} mol·dm^{-3} of SH-BTPM, as well as the as-polished surface imaging. As observed in Fig. 12 (e), the SEM image denotes that the entire surface of the N80 carbon steel is severely corroded and has numerous corrosion pits that started to appear on the surface in only 1 mol·dm^{-3} HCl with no additives, with reference to the as-polished sample in Fig. 12 (d). The EDX chart in Fig. 12 (b) reveals that oxygen atoms exhibit a large peak related to the oxidation of the N80 carbon steel surface as a result of the exposure to the corrosive medium with reference to free polished sample chart in Fig. 12 (a).

By contrast, the SEM image depicted in Fig. 12 (f) reveals that the entire carbon steel surface exhibited a significantly smoother

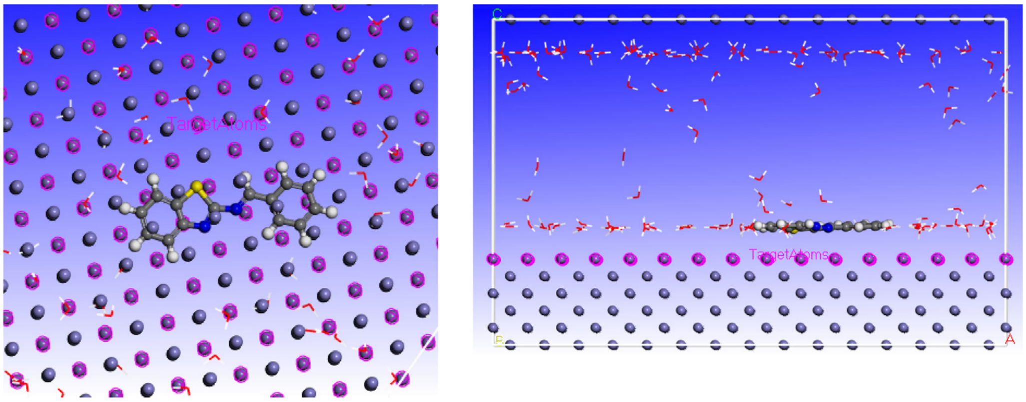

Top view Side view

(a) H-BTPM

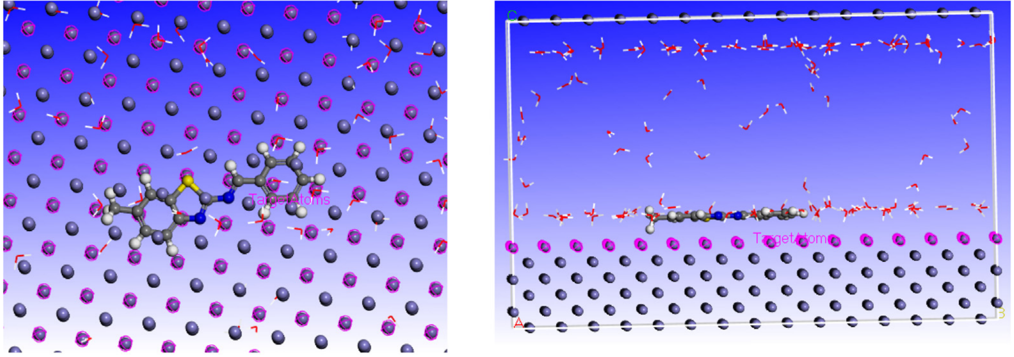

Top view Side view

(b) Me-BTPM

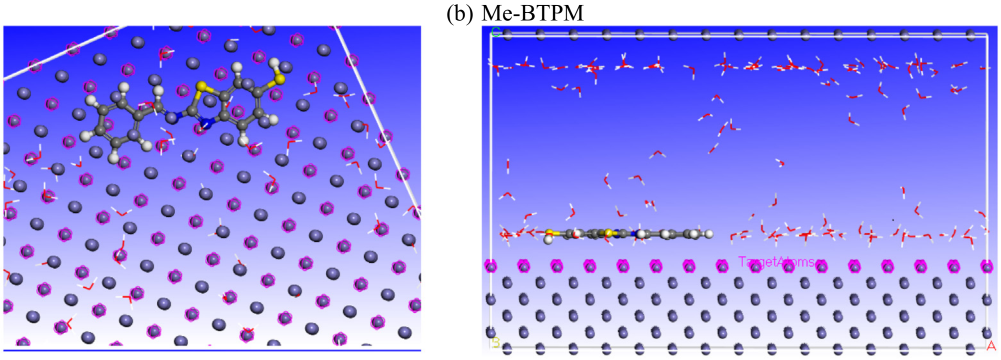

Top view Side view

(c) SH-BTPM

Fig. 10. Simulated adsorption of BTPM series inhibitors over Fe (1 0 0) surface using adsorption locator module.

Table 6
Calculated energy descriptors using Mont Carlo simulations for the adsorption of BTPM series compounds on Fe (1 0 0) surface.

Inhibitor	Total energy	Adsorption energy	Rigid adsorption energy	Deformation energy	Inhibitor : dE_{ad}/dN_i	Water : dE_{ad}/dN_i
H-BTPM	−1799.56	−1769.24	−1824.88	55.63	−123.16	−0.57
Me-BTPM	−1818.03	−1778.49	−1834.48	55.98	−125.60	−0.58
SH-BTPM	−1838.00	−1799.67	−1854.80	55.1	−144.57	−0.48

texture after adding 1 × 10^{-2} mol·dm^{-3} of SH-BTPM to the 1 mol·dm^{-3} HCl medium with residual inhibitor molecule clusters present on the surface. As shown by the corresponding EDX chart in Fig. 12 (c), almost no oxygen peak was detected, indicating the elimination of any surface oxidation reaction. In parallel, a significant decrease in the iron peak intensity was observed in Fig. 12 (c) in comparison with the as-polished and corroded samples, indicating the shielding effect of the formed layer of the SH-BTPM inhibitor. Therefore, these findings strongly attest to the prominent performance of the BTPM series as anticorrosion additives for N80 carbon steel in 1 mol·dm^{-3} HCl medium [129–133].

3.8. Atomic force microscope morphological studies

Atomic force microscope (AFM) analysis is a robust technique used to assess the morphological surface alterations for the used substrate before and after the addition of corrosion inhibitors.

Table 7
Antibacterial activity of the synthesized BTPM series in term of inhibition zone diameter[*].

Compounds	Diameter inhibition zone in mm (% activity index)			
	Gram-positive bacteria		Gram-negative bacteria	
	Bacillus subtilis (ATCC 6633)	Staphylococcus aureus (ATCC 29737)	Pseudomonas aeruginosa (ATCC 9027)	Escherichia coli (ATCC 8739)
H-BTPM	14(70)	15(65)	12(67)	14(78)
Me-BTPM	18(90)	22(95)	15(83)	16(89)
SH-BTPM	24(120)	27(117)	20(111)	22(122)
[**]TE (30 mcg)	20(100)	23(100)	–	–
[**]NA (30 mcg)	–	–	18(100)	18(100)

[*] Standard deviation = 5%, [**]TE: Tetracycline, NA: Nalidixic acid.

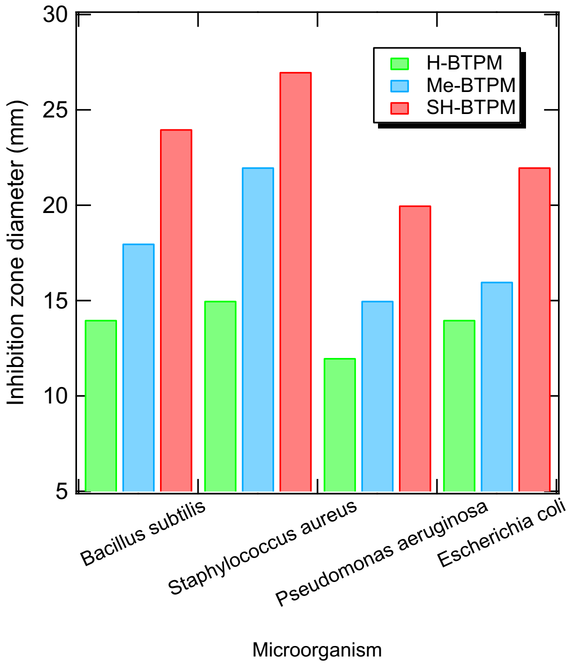

Fig. 11. Anti-bacterial activity of the synthesized benzothiazole derivatives against different microorganism.

Fig. 13 depicts the AFM 3D images of the N80 carbon steel surface after 24 h immersion at room temperature in 1 mol·dm^{-3} HCl. As shown in Fig. 13 (a), the carbon steel surface was coarsened and severely damaged by the effect of only 1 mol·dm^{-3} HCl solution. Fig. 13 (b) depicts the 3D imaging of the N80 carbon steel surface after being introduced to the SH-PTBM inhibitor in the same acidic solution. After the addition of the SH-PTBM inhibitor, the entire surface of the N80 carbon steel became flatter and smoother due to the isolation of the entire surface by an SH-PTBM layered protective film [134,135].

3.9. Corrosion inhibition mechanism

As reported in this study, the BTPM series molecules were adsorbed to the N80 carbon steel surface using mutual physical and chemical interactions in 1 mol·dm^{-3}HCl. The charge of the metal surface can be determined from the value of $E_{corr} - E_q = 0$ (zero charge potential (vs. SCE). *Xianghong Li* [136] reported that the value of $E_q = 0$ of iron is −530 mV versus SCE in HCl. In the present study, the value of E_{corr} obtained in 1 mol·dm^{-3}HCl is −514 mV. Therefore, the charges of steel surface is positive charge in HCl because of $E_{corr} - E_q > 0$. Since the negative ions of Cl^- could be specifically adsorbed firstly on the metal surface, they create excess negatives charge towards the solution and favor more adsorption of the inhibitor cations. The protonated BTPM series molecules can adsorp physically at the negative Cl^- iond and restrict the passage of other corrosive ions towards the interior steel surface which inhibit the corrosion process [137]. The suggested corrosion inhibition mechanism possessed by the BTPM derivatives regarding the carbon steel surface is schematically explained in Fig. 14. On the other hand, these derivatives can be adsorbed chemically onto the steel surface through their high electron density cloud, due to structural factors emerging from their possession of S, N heteroatoms, π-electrons of aromatic cycles, and the imine group (—C═N—) that helped to extend the double bond conjugation throughout the whole structure causing better electron distribution and a more planar conformation on the substrate surface [138]. Therefore, the chemical adsorption was possible via the coordinating bonds between the lone electron pairs of the inhibitor molecules and the empty *d*-orbitals of the N80 carbon steel surface [139].

The variation between the three BTPM series molecules (H-BTPM, Me-BTPM, and SH-BTPM) in terms of their chemical structure, was responsible for their different corrosion inhibition performance, as reported throughout all this study. Examining these structural deviations, the Me-BTPM molecule possessed a methyl substitute group, and SH-BTPM possessed a thiol group while H-BTPM didn't contain any substituents. The methyl substituent in Me-BTPM is electron-releasing, which can increase the electron density towards the structure and accordingly it boosted the inhibition efficiency from 75% to 82% regarding H-BTPM. Moreover,

Table 8
Minimum inhibitory concentrations (MICs) and minimum bactericidal concentrations (MBCs) of the synthesized BTPM series against different standard bacterial strains.

Compounds	Bacterial strains							
	Bacillus subtilis (ATCC 6633)		Staphylococcus aureus (ATCC 29737)		Pseudomonas aeruginosa (ATCC 9027)		Escherichia coli (ATCC 8739)	
	MIC[*] (μM)	MBC[**] (μM)	MIC[*] (μM)	MBC[**] (μM)	MIC[*] (μM)	MBC[**] (μM)	MIC[*] (μM)	MBC[**] (μM)
H-BTPM	31.2	43.7	21.8	37.5	43.7	62.5	37.5	46.8
Me-BTPM	21.8	31.2	15.6	28.1	31.2	38.5	25.0	34.5
SH-BTPM	6.25	9.35	9.35	12.5	15.6	25.0	12.5	18.7

[*] MIC = Minimum inhibitory concentration, [**]MBC = Minimum bactericidal concentration.

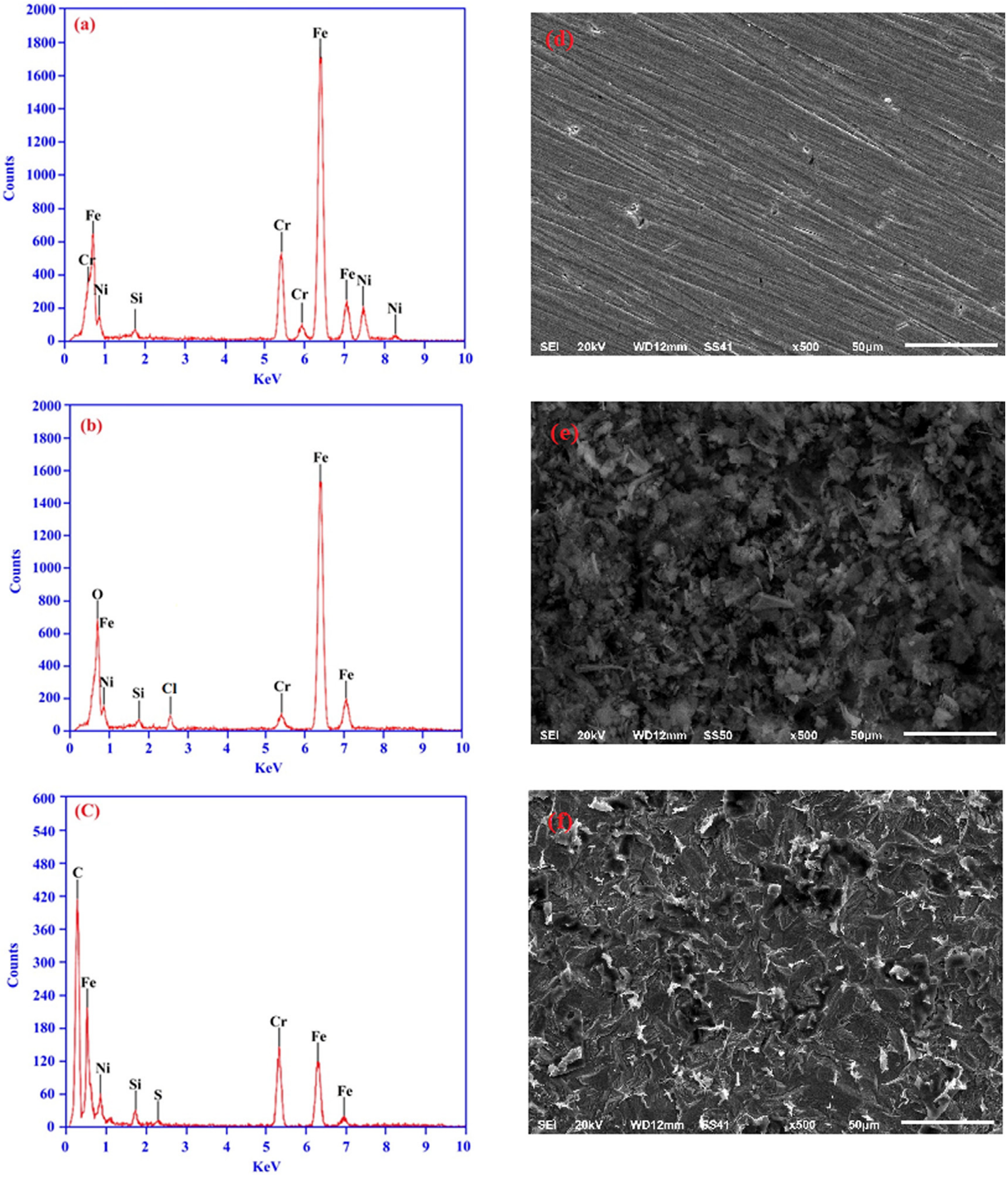

Fig. 12. SEM & EDX charts of the carbon steel sample: (a), (d) EDX and SEM for free polished surface (b), (e) EDX and SEM for the surface after 24 h immersion at room temperature in 1 mol $dm^{-3}HCl$ (c), (f) EDX and SEM for the surface after 24 h immersion at room temperature in 1 mol $dm^{-3}HCl$ with 1×10^{-2} of SH-PTBM inhibitor.

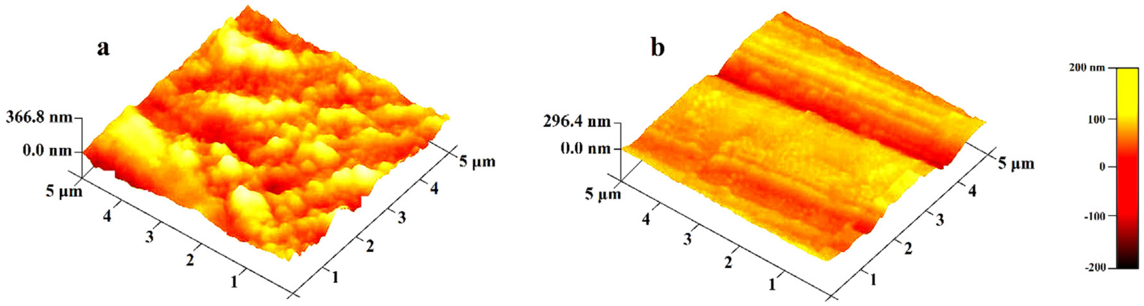

Fig. 13. AFM morphology of carbon steel surface before and after 24 h immersion at room temperature in 1 mol $dm^{-3}HCl$ (a) without and (b) with 1×10^{-2} of SH-PTBM inhibitor.

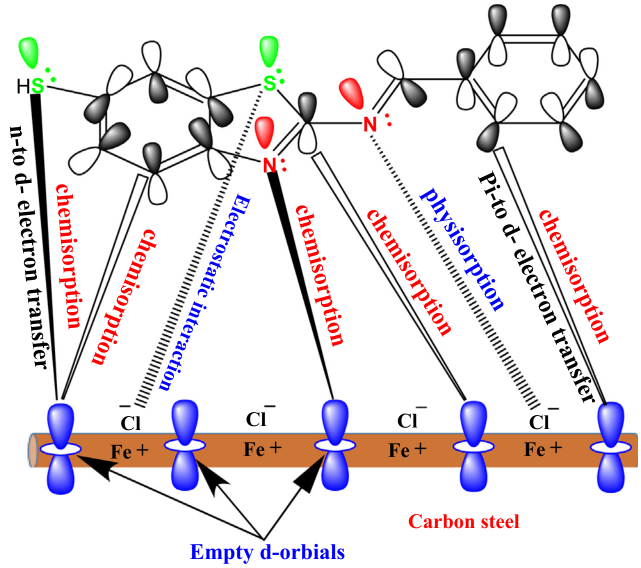

Fig. 14. Possible adsorption mechanism of SH-PTBM on the carbon steel surface in HCl solution.

SH-BTPM which recorded the highest inhibition efficiency of 90%, possessed a thiol group (—SH) with its two unshared pairs of electrons, which enhanced the possibilities of direct coordination to the N80 carbon steel surface [140]. Consequently, these benzothiazole derivatives can form a protective adsorbed layer onto the surface of N80 carbon steel by physical and chemical means of interaction, isolating the carbon steel from further dissolution. Fig. 14 represented the graphical representation of the adsorption mechanism with emphasizing the possible different interactions between SH-BTPM and the carbon steel surface.

3.10. Comparison of inhibitive effect with other benzothiazole derivatives

The inhibition efficiencies of the investigated BTPM series were compared with similar type literature survey of benzothiazoles inhibitors. Table 9 listed a comparative inhibition efficiencies of various benzothiazole derivatives at ambient temperature [141–146]. It can be seen that the investigated BTPM series used in the present study give higher inhibition efficiency compared to most of previously reported benzotriazole derivatives. This is related to the similarity in their structure and intrinsic molecular properties, which has led towards comparable extent of interaction with the carbon steel.

4. Conclusions

1. Three new structurally designed benzothiazole derivatives namely; SH-BTPM, Me-BTPM, and H-BTPM, were successively synthesized, confirmed by FTIR and NMR analyses, and were studied for their anticorrosion behavior against HCl solution on N80 carbon steel solution using chemical and electrochemical techniques, besides, they were studied as biocides against some bacterial strains proven for causing microbially influenced corrosion.
2. The BTPM series behaved as mixed-type inhibitors, and a corrosion inhibition efficiency of 90% was obtained in the presence of 1×10^{-2} mol·dm^{-3}SH-BTPM in 1 mol·dm^{-3} (~3.1%) HCl solution that is used in shale formation well acidization.
3. The inhibitive action of the BTPM series was attributed to their strong adsorption to the metal surface in alignment with the Langmuir adsorption module.
4. Surface morphology images of SEM, EDX, and AFM test indicated the formation of an isolative layer on the N80 carbon steel in HCl solution.
5. The BTPM series displayed a broad-spectrum antibacterial activity against Gram-positive and Gram-negative bacteria that may induce bacterial corrosion, in comparison with standard antibiotics.
6. The biocidal efficacy of BTPM series molecules powerfully associated with the existence of the benzothiazole ring nucleus, and the azomethine group(—C=Nsbnd) in their chemical structures.
7. DFT calculations evinced the ability of the BTPM series ability to work as potential inhibitors due to the comparatively low ΔE_{Gap} values. Besides, MC simulations showed the planarity of the inhibitor molecules on the Fe surface due to its unique structure.
8. Further studies are needed such as X-ray Photoelectron Spectroscopy (XPS) in order to investigate the species and ions that formed on the surface before and after the application of the BTPM series inhibitors. In addition to the study of the effect of pitting exerted by chloride ions.

Table 9
Comparative table on inhibition efficiencies of various benzothiazole derivatives at ambient temperature.

Benzothiazole inhibitor	Concentration	Corrosive system	η (%)	Reference
1,3-Benzothiazol-2-amine (BTA)	0.33 mM	Mild steel in 1 M HCl	67	[141]
6-Methyl-1,3-benzothiazol-2-amine	0.30 mM		72	
2-Amino-1,3-benzthiazole-6-thiol	0.22 mM		76	
2-Aminobenzothiazole (ABT)	2 mM	Carbon steel in 1 M HCl	75	[142]
2-Mercaptobenzothiazole			86	
Benzothiazole-2-amine	1 mM	Mild steel in 1 M H_2SO_4	59	[143]
Benzothiazole-2-yl-thiocarbohydrazide			69	
Benzothiazole-2-yl-thiosemicarbazide			87	
2-(2′-Hydroxylphenyl)benzothiazole	0.22 mM	Mild steel in 1 M HCl	85	[144]
2-(2′,5′-Dihydroxyphenyl)benzothiazole	0.20 mM		45	
(4-Benzothiazole-2-yl-phenyl)-dimethyl-amine	0.19 mM		95	
2-Mercaptobenzothiazole	1 mM	Carbon steel in 1 M HCl	40	[145]
2-(n-hexylamino)-4-(3′-N,N-dimethylamino-propyl)amino-6-(benzothiazol-2-yl)thio-1,3,5-s-triazine			96	
2-(n-octylamino)-4-(3′-N,N-dimethylamino-propyl)amino-6-(benzothiazol-2-yl)thio-1,3,5-s-triazine			97	
1,2-Bis-(2-benzimidazolyl) ethylene	1 mM	Mild steel in 1 M HCl	89	[146]
Bis-(2-benzimidazolyl methyl) oxide			91	
Bis-(2-benzimidazolyl methyl) sulphide			92	
2,6-Bis-(2-benzimidazolyl) pyridine			96	

CRediT authorship contribution statement

Ahmed A. Farag: Methodology, Investigation, Validation, Writing - original draft. **A.M. Eid:** Software, Formal analysis, Data curation, Validation, Writing - review & editing. **M.M. Shaban:** Resources, Methodology, Validation. **Eslam A. Mohamed:** Writing - review & editing, Validation. **Gunasunderi Raju:** Supervision, Resources, Methodology.

Declaration of Competing Interest

The authors declare that they have no known competing financial interests or personal relationships that could have appeared to influence the work reported in this paper.

Acknowledgment

The authors are greatly thankful to the Egyptian Petroleum Research Institute (EPRI) and Universiti Sains Malaysia (USM) for funding and support.

References

[1] M. Iannuzzi, A. Barnoush, R. Johnsen, Materials and corrosion trends in offshore and subsea oil and gas production, npj Mater. Degrad. 1 (2017) 1–11.

[2] R. Heidersbach, Metallurgy and Corrosion Control in Oil and Gas Production, John Wiley & Sons, 2018.

[3] A.A. Olajire, Corrosion inhibition of offshore oil and gas production facilities using organic compound inhibitors-A review, J. Mol. Liq. 248 (2017) 775–808.

[4] A.M. El Defrawy, M. Abdallah, J.H. Al-Fahemi, Electrochemical and theoretical investigation for some pyrazolone derivatives as inhibitors for the corrosion of C-steel in 0.5 M hydrochloric acid, J. Mol. Liq. 288 (2019), https://doi.org/10.1016/j.molliq.2019.110994.

[5] M. Abdallah, H.M. Altass, A.S. Al-Gorair, J.H. Al-Fahemi, B.A.A.L. Jahdaly, K.A. Soliman, Natural nutmeg oil as a green corrosion inhibitor for carbon steel in 1.0 M HCl solution: Chemical, electrochemical, and computational methods, J. Mol. Liq. 323 (2021), https://doi.org/10.1016/j.molliq.2020.115036.

[6] R.S.A. Hameed, E.H. Aljuhani, A.H. Al-Bagawi, A.H. Shamroukh, M. Abdallah, Study of sulfanyl pyridazine derivatives as efficient corrosion inhibitors for carbon steel in 1.0 m hcl using analytical techniques, Int. J. Corros. Scale Inhib. 9 (2020) 623–643. https://doi.org/10.17675/2305-6894-2020-9-2-16.

[7] M. Alfakeer, M. Abdallah, A. Fawzy, Corrosion inhibition effect of expired ampicillin and flucloxacillin drugs for mild steel in aqueous acidic medium, Int. J. Electrochem. Sci. 15 (2020) 3283–3297. https://doi.org/10.20964/2020.04.09.

[8] M. Mobin, M. Basik, J. Aslam, Boswellia serrata gum as highly efficient and sustainable corrosion inhibitor for low carbon steel in 1 M HCl solution: Experimental and DFT studies, J. Mol. Liq. 263 (2018) 174–186, https://doi.org/10.1016/j.molliq.2018.04.150.

[9] M. Pakiet, I.H. Kowalczyk, R. Leiva Garcia, R. Akid, B.E. Brycki, Influence of different counterions on gemini surfactants with polyamine platform as corrosion inhibitors for stainless steel AISI 304 in 3 M HCl, J. Mol. Liq. 268 (2018) 824–831, https://doi.org/10.1016/j.molliq.2018.07.120.

[10] O. Kaczerewska, R. Leiva-Garcia, R. Akid, B. Brycki, I. Kowalczyk, T. Pospieszny, Effectiveness of O-bridged cationic gemini surfactants as corrosion inhibitors for stainless steel in 3M HCl: Experimental and theoretical studies, J. Mol. Liq. 249 (2018) 1113–1124, https://doi.org/10.1016/j.molliq.2017.11.142.

[11] F.A. Azeez, O.A. Al-Rashed, A.A. Nazeer, Controlling of mild-steel corrosion in acidic solution using environmentally friendly ionic liquid inhibitors: Effect of alkyl chain, J. Mol. Liq. 265 (2018) 654–663, https://doi.org/10.1016/j.molliq.2018.05.093.

[12] A. Salhi, S. Tighadouini, M. El-Massaoudi, M. Elbelghiti, A. Bouyanzer, S. Radi, S. El Barkany, F. Bentiss, A. Zarrouk, Keto-enol heterocycles as new compounds of corrosion inhibitors for carbon steel in 1M HCl: Weight loss, electrochemical and quantum chemical investigation, J. Mol. Liq. 248 (2017) 340–349, https://doi.org/10.1016/j.molliq.2017.10.040.

[13] H. Behzadi, A. Forghani, Correlation between electronic parameters and corrosion inhibition of benzothiazole derivatives- NMR parameters as important and neglected descriptors, J. Mol. Struct. 1131 (2017) 163–170, https://doi.org/10.1016/j.molstruc.2016.11.037.

[14] A.A. Farag, Applications of nanomaterials in corrosion protection coatings and inhibitors, Corros. Rev. 38 (2020) 67–86, https://doi.org/10.1515/corrrev-2019-0011.

[15] A.A. Farag, A.S. Ismail, M.A. Migahed, Environmental-friendly shrimp waste protein corrosion inhibitor for carbon steel in 1 M HCl solution, Egypt. J. Pet. (2018), https://doi.org/10.1016/j.ejpe.2018.05.001.

[16] P.E. Alvarez, M.V. Fiori-Bimbi, A. Neske, S.A. Brandán, C.A. Gervasi, Rollinia occidentalis extract as green corrosion inhibitor for carbon steel in HCl solution, J. Ind. Eng. Chem. 58 (2018) 92–99, https://doi.org/10.1016/j.jiec.2017.09.012.

[17] M. Cui, S. Ren, H. Zhao, L. Wang, Q. Xue, Novel nitrogen doped carbon dots for corrosion inhibition of carbon steel in 1 M HCl solution, Appl. Surf. Sci. 443 (2018) 145–156, https://doi.org/10.1016/j.apsusc.2018.02.255.

[18] H.A. Mohamed, A.A. Farag, B.M. Badran, Friendly to environment heterocyclic adducts as corrosion inhibitors for steel in water-borne paints, J. Appl. Polym. Sci. 117 (2010) 1270–1278, https://doi.org/10.1002/app.31838.

[19] B.M.B.H.A. Mohamed, A.A. Farag, Corrosion inhibition of mild steel using emulsified thiazole adduct in Different binder systems, Eurasian Chem. 10 (2008) 67–77.

[20] Z. Salarvand, M. Amirnasr, M. Talebian, K. Raeissi, S. Meghdadi, Enhanced corrosion resistance of mild steel in 1 M HCl solution by trace amount of 2-phenyl-benzothiazole derivatives: Experimental, quantum chemical calculations and molecular dynamics (MD) simulation studies, Corros. Sci. 114 (2017) 133–145, https://doi.org/10.1016/j.corsci.2016.11.002.

[21] H.M. Abd El-Lateef, Experimental and computational investigation on the corrosion inhibition characteristics of mild steel by some novel synthesized imines in hydrochloric acid solutions, Corros. Sci. 92 (2015) 104–117, https://doi.org/10.1016/j.corsci.2014.11.040.

[22] B. Tan, S. Zhang, Y. Qiang, L. Feng, C. Liao, Y. Xu, S. Chen, Investigation of the inhibition effect of Montelukast Sodium on the copper corrosion in 0.5mol/L H2SO4, J. Mol. Liq. 248 (2017) 902–910, https://doi.org/10.1016/j.molliq.2017.10.111.

[23] C. Verma, I.B. Obot, I. Bahadur, E.-S.M. Sherif, E.E. Ebenso, Choline based ionic liquids as sustainable corrosion inhibitors on mild steel surface in acidic medium: Gravimetric, electrochemical, surface morphology, DFT and Monte Carlo simulation studies, Appl. Surf. Sci. 457 (2018) 134–149, https://doi.org/10.1016/j.apsusc.2018.06.035.

[24] X. Zheng, S. Zhang, W. Li, M. Gong, L. Yin, Experimental and theoretical studies of two imidazolium-based ionic liquids as inhibitors for mild steel in sulfuric acid solution, Corros. Sci. 95 (2015) 168–179, https://doi.org/10.1016/j.corsci.2015.03.012.

[25] X. Zhou, H. Yang, F. Wang, [BMIM]BF4 ionic liquids as effective inhibitor for carbon steel in alkaline chloride solution, Electrochim. Acta 56 (2011) 4268–4275, https://doi.org/10.1016/j.electacta.2011.01.081.

[26] P. Huang, J.-A. Latham, D.R. MacFarlane, P.C. Howlett, M. Forsyth, A review of ionic liquid surface film formation on Mg and its alloys for improved corrosion performance, Electrochim. Acta 110 (2013) 501–510, https://doi.org/10.1016/j.electacta.2013.03.097.

[27] N. Yilmaz, A. Fitoz, ÿmit Ergun, K.C. Emregül, A combined electrochemical and theoretical study into the effect of 2-((thiazole-2-ylimino)methyl)phenol as a corrosion inhibitor for mild steel in a highly acidic environment, Corros. Sci. 111 (2016) 110–120, https://doi.org/10.1016/j.corsci.2016.05.002.

[28] H. Hamani, T. Douadi, D. Daoud, M. Al-Noaimi, R.A. Rikkouh, S. Chafaa, 1-(4-Nitrophenylo-imino)-1-(phenylhydrazono)-propan-2-one as corrosion inhibitor for mild steel in 1M HCl solution: Weight loss, electrochemical, thermodynamic and quantum chemical studies, J. Electroanal. Chem. 801 (2017) 425–438, https://doi.org/10.1016/j.jelechem.2017.08.031.

[29] D.K. Singh, E.E. Ebenso, M.K. Singh, D. Behera, G. Udayabhanu, R.P. John, Non-toxic Schiff bases as efficient corrosion inhibitors for mild steel in 1M HCl: Electrochemical, AFM, FE-SEM and theoretical studies, J. Mol. Liq. 250 (2018) 88–99, https://doi.org/10.1016/j.molliq.2017.11.132.

[30] J. Chauhan, W. Yu, S. Cardinale, T.J. Opperman, A.D. MacKerell Jr, S. Fletcher, E.P.H. de Leeuw, Optimization of a Benzothiazole Indolene Scaffold Targeting Bacterial Cell Wall Assembly, Drug Des. Devel. Ther. 14 (2020) 567.

[31] C.B.C. Ikpa, S.O. Onoja, A.O. Okwaraji, Synthesis And Antibacterial Activities Of Benzothiazole Derivatives Of Sulphonamides, Acta Chem. Malaysia. 4 (2020) 55–57.

[32] F. Viani, B. Rossi, W. Panzeri, L. Merlini, A.M. Martorana, A. Polissi, Y.M. Galante, Synthesis and anti-bacterial activity of a library of 1,2-benzisothiazol-3(2H)-one (BIT) derivatives amenable of crosslinking to polysaccharides, Tetrahedron 73 (2017) 1745–1761, https://doi.org/10.1016/j.tet.2017.02.025.

[33] R.A. Daly, M.A. Borton, M.J. Wilkins, D.W. Hoyt, D.J. Kountz, R.A. Wolfe, S.A. Welch, D.N. Marcus, R.V. Trexler, J.D. MacRae, Microbial metabolisms in a 2.5-km-deep ecosystem created by hydraulic fracturing in shales, Nat. Microbiol. 1 (2016) 1–9.

[34] A. Murali Mohan, A. Hartsock, R.W. Hammack, R.D. Vidic, K.B. Gregory, Microbial communities in flowback water impoundments from hydraulic fracturing for recovery of shale gas, FEMS Microbiol. Ecol. 86 (2013) 567–580.

[35] N.A. Negm, M.A. Migahed, R.K. Farag, A.A. Fadda, M.K. Awad, M.M. Shaban, High performance corrosion inhibition of novel tricationic surfactants on carbon steel in formation water: Electrochemical and computational evaluations, J. Mol. Liq. 262 (2018) 363–375, https://doi.org/10.1016/j.molliq.2018.04.092.

[36] J. Wang, B. Hou, J. Xiang, X. Chen, T. Gu, H. Liu, The performance and mechanism of bifunctional biocide sodium pyrithione against sulfate reducing bacteria in X80 carbon steel corrosion, Corros. Sci. 150 (2019) 296–308, https://doi.org/10.1016/j.corsci.2019.01.037.

[37] N. Kovačević, A. Kokalj, DFT Study of Interaction of Azoles with Cu(111) and Al(111) Surfaces: Role of Azole Nitrogen Atoms and Dipole-Dipole Interactions, J. Phys. Chem. C 115 (2011) 24189–24197, https://doi.org/10.1021/jp207076w.

[38] A.H. El-Askalany, S.I. Mostafa, K. Shalabi, A.M. Eid, S. Shaaban, Novel tetrazole-based symmetrical diselenides as corrosion inhibitors for N80

carbon steel in 1 M HCl solutions: Experimental and theoretical studies, J. Mol. Liq. 223 (2016) 497–508, https://doi.org/10.1016/j.molliq.2016.08.088.
[39] F.J. Rodríguez-Gómez, M.P. Valdelamar, A.E. Vazquez, P. Del Valle Perez, R. Mata, A. Miralrio, M. Castro, Mycophenolic acid as a corrosion inhibitor of carbon steel in 3% wt. NaCl solution. An experimental and theoretical study, J. Mol. Struct. 1183 (2019) 168–181, https://doi.org/10.1016/j.molstruc.2018.12.035.
[40] G. Bahlakeh, B. Ramezanzadeh, M. Ramezanzadeh, Cerium oxide nanoparticles influences on the binding and corrosion protection characteristics of a melamine-cured polyester resin on mild steel: An experimental, density functional theory and molecular dynamics simulation study, Corros. Sci. 118 (2017) 69–83, https://doi.org/10.1016/j.corsci.2017.01.021.
[41] J.M. Mir, R.C. Maurya, P.K. Vishwakarma, Corrosion resistance and thermal behavior of acetylacetonato-oxoperoxomolybdenum(VI) complex of maltol: Experimental and DFT studies, Karbala Int. J. Mod. Sci. 3 (2017) 212–223, https://doi.org/10.1016/j.kijoms.2017.08.006.
[42] E.E. Oguzie, Y. Li, S.G. Wang, F. Wang, Understanding corrosion inhibition mechanisms—experimental and theoretical approach, RSC Adv. 1 (2011) 866, https://doi.org/10.1039/c1ra00148e.
[43] H. Ke, C.D. Taylor, Density Functional Theory: An Essential Partner in the Integrated Computational Materials Engineering Approach to Corrosion, CORROSION. 75 (2019) 708–726, https://doi.org/10.5006/3050.
[44] C. Verma, M.A. Quraishi, E.E. Ebenso, Microwave and ultrasound irradiations for the synthesis of environmentally sustainable corrosion inhibitors: An overview, Sustain. Chem. Pharm. 10 (2018) 134–147, https://doi.org/10.1016/j.scp.2018.11.001.
[45] C.G.M. Hermse, A.P. van Bavel, A.P.J. Jansen, L.A.M.M. Barbosa, P. Sautet, R.A. van Santen, Formation of Chiral Domains for Tartaric Acid on Cu(110): A Combined DFT and Kinetic Monte Carlo Study, J. Phys. Chem. B 108 (2004) 11035–11043, https://doi.org/10.1021/jp0490195.
[46] C. Whitby, Oilfield Microbiology (2019), https://doi.org/10.1201/9781315164700.
[47] G.J. Schmitz, U. Prahl, Handbook of Software Solutions for ICME (2016), https://doi.org/10.1002/9783527693566.
[48] J. Sheng, S. Morsy, A. Gomaa, M.Y. Soliman, Matrix acidizing characteristics in shale formations, J. Pet. Environ. Biotechnol. 5 (2014) 1.
[49] S.S. Morsy, J.J. Sheng, M.Y. Soliman, Improving hydraulic fracturing of shale formations by acidizing, in: SPE East. Reg. Meet., Society of Petroleum Engineers, 2013.
[50] T. Guo, Y. Li, Y. Ding, Z. Qu, N. Gai, Z. Rui, Evaluation of acid fracturing treatments in shale formation, Energy Fuels 31 (2017) 10479–10489.
[51] C. Lu, L. Ma, J. Guo, S. Xiao, Y. Zheng, C. Yin, Effect of acidizing treatment on microstructures and mechanical properties of shale, Nat. Gas Ind. B (2020).
[52] R. Liang, I.A. Davidova, C.R. Marks, B.W. Stamps, B.H. Harriman, B.S. Stevenson, K.E. Duncan, J.M. Suflita, Metabolic capability of a predominant Halanaerobium sp. in hydraulically fractured gas wells and its implication in pipeline corrosion, Front. Microbiol. 7 (2016) 988.
[53] M. Demeter, V. Wornstaff, C. Wiggins, D. Maley, A Comprehensive Microbial Assessment of Hydraulic Fracturing Stimulations using State-of-The-Art Molecular Methods: Three Western-Canadian Case Studies, in, SPE Annu. Tech. Conf. Exhib., Society of Petroleum Engineers (2019).
[54] W.T. Stringfellow, M.K. Camarillo, J.K. Domen, W.L. Sandelin, C. Varadharajan, P.D. Jordan, M.T. Reagan, H. Cooley, M.G. Heberger, J.T. Birkholzer, Identifying chemicals of concern in hydraulic fracturing fluids used for oil production, Environ. Pollut. 220 (2017) 413–420.
[55] M. Lebrini, F. Bentiss, N.-E. Chihib, C. Jama, J.P. Hornez, M. Lagrenée, Polyphosphate derivatives of guanidine and urea copolymer: inhibiting corrosion effect of Armco iron in acid solution and antibacterial activity, Corros. Sci. 50 (2008) 2914–2918.
[56] H.Z. Wadood, A. Rajasekar, Y.-P. Ting, A.N. Sabari, Role of Bacillus subtilis and Pseudomonas aeruginosa on corrosion behaviour of stainless steel, Arab. J. Sci. Eng. 40 (2015) 1825–1836.
[57] I. Neria-González, E.T. Wang, F. Ramírez, J.M. Romero, C. Hernández-Rodríguez, Characterization of bacterial community associated to biofilms of corroded oil pipelines from the southeast of Mexico, Anaerobe. 12 (2006) 122–133.
[58] M. Chylińska, H. Kaczmarek, A. Burkowska-But, Preparation and characteristics of antibacterial chitosan films modified with N-halamine for biomedical application, Colloids Surfaces B Biointerfaces. 176 (2019) 379–386, https://doi.org/10.1016/j.colsurfb.2019.01.013.
[59] R.A. Miller, R.D. Walker, J. Carson, M. Coles, R. Coyne, I. Dalsgaard, C. Gieseker, H.M. Hsu, J.J. Mathers, B.P.M. Papapetropoulou, C. Teitzel, Standardization of a broth microdilution susceptibility testing method to determine minimum inhibitory concentrations of aquatic bacteria, Dis. Aquat. Organ. 64 (2005) 211–222.
[60] M. Jadhav, R.S. Kalhapure, S. Rambharose, C. Mocktar, T. Govender, Synthesis, characterization and antibacterial activity of novel heterocyclic quaternary ammonium surfactants, J. Ind. Eng. Chem. 47 (2017) 405–414, https://doi.org/10.1016/j.jiec.2016.12.013.
[61] ISO 9226, 2012. Corrosion of metals and alloys.
[62] Adsorption and inhibition behavior of a novel Schiff base on carbon steel corrosion in acid media, n.d.
[63] Z. Hu, Y. Meng, X. Ma, H. Zhu, J. Li, C. Li, D. Cao, Experimental and theoretical studies of benzothiazole derivatives as corrosion inhibitors for carbon steel in 1 M HCl, Corros. Sci. 112 (2016) 563–575, https://doi.org/10.1016/j.corsci.2016.08.012.
[64] K.M. Shainy, P.R. Ammal, A. Joseph, Development of passive film and enhancement of corrosion protection of mild steel in hydrochloric acid through the synergistic interaction of 2-amino-4-methyl benzothiazole (AMBT) and (E) -2-methylbenzo [d] thiazol-2-yl) imino-4-methyl) phenol (MBTP), Egypt. J. Pet. 27 (2018) 621–632, https://doi.org/10.1016/j.ejpe.2017.09.004.
[65] K. Shalabi, Y.M. Abdallah, A.S. Fouda, Corrosion inhibition of aluminum in 0.5 M HCl solutions containing phenyl sulfonylacetophenoneazo derivatives, Res. Chem. Intermed. 41 (2014) 4687–4711, https://doi.org/10.1007/s11164-014-1561-5.
[66] B.E.-D.M. El-Gendy, S.T. Atwa, A.A. Ahmed, A.Y. El-Etre, Synthesis and Characterization of Carbon Steel Corrosion Inhibitors Based on 4,5,6,7-tetrahydrobenzo[b]thiophene Scaffold, Prot. Met. Phys. Chem. Surfaces. 55 (2019) 179–186, https://doi.org/10.1134/s2070205119010106.
[67] A. Rojas, S. Cabal, G.A. Papadantonakis, A theoretical investigation of sugar and phosphate contributions to the activation barriers of guanine methylation by carcinogenic methane diazonium ion, Chem. Phys. Lett. 714 (2019) 24–29, https://doi.org/10.1016/j.cplett.2018.10.063.
[68] D.E. Jiang, E.A. Carter, Adsorption and diffusion energetics of hydrogen atoms on Fe(110) from first principles, Surf. Sci. 547 (2003) 85–98, https://doi.org/10.1016/j.susc.2003.10.007.
[69] F. Radjai, C. Voivret, Periodic boundary conditions, n.d.
[70] Inhibition of carbon steel corrosion in acidic solution using some newly polyester derivatives, n.d.
[71] A.A. Farag, M.A. Hegazy, Synergistic inhibition effect of potassium iodide and novel Schiff bases on X65 steel corrosion in 0.5M H2SO4, Corros. Sci. 74 (2013) 168–177, https://doi.org/10.1016/j.corsci.2013.04.039.
[72] M.A. Migahed, A.A. Farag, S.M. Elsaed, R. Kamal, M. Mostfa, H.A. El-Bary, Synthesis of a new family of Schiff base nonionic surfactants and evaluation of their corrosion inhibition effect on X-65 type tubing steel in deep oil wells formation water, Mater. Chem. Phys. (2011), https://doi.org/10.1016/j.matchemphys.2010.08.082.
[73] X. Li, S. Deng, X. Xie, Experimental and theoretical study on corrosion inhibition of oxime compounds for aluminium in HCl solution, Corros. Sci. 81 (2014) 162–175, https://doi.org/10.1016/j.corsci.2013.12.021.
[74] O.L. Riggs Jr., Corrosion Inhibitors, second ed., TXNACE (National Association of Corrosion Engineers), TX, Houston, 1973.
[75] N.A. Migahed, M.A. Shaban, M.M. Fadda, A.A. Ali, T.A. Negm, Synthesis of some quaternary ammonium gemini surfactants and evaluation of their performance as corrosion inhibitors for carbon steel in oil well formation water containing sulfide ions, RSC Adv. 5 (2015) 104480–104492.
[76] The adsorption and corrosion inhibition of some nonionic surfactants on API X65 steel surface in hydrochloric acid, n.d.
[77] J. Saranya, M. Sowmiya, P. Sounthari, K. Parameswari, S. Chitra, K. Senthilkumar, N-heterocycles as corrosion inhibitors for mild steel in acid medium, J. Mol. Liq. 216 (2016) 42–52, https://doi.org/10.1016/j.molliq.2015.12.096.
[78] S. Deng, X. Li, X. Xie, Hydroxymethyl urea and 1,3-bis(hydroxymethyl) urea as corrosion inhibitors for steel in HCl solution, Corros. Sci. 80 (2014) 276–289, https://doi.org/10.1016/j.corsci.2013.11.041.
[79] D. Daoud, T. Douadi, S. Issaadi, S. Chafaa, Adsorption and corrosion inhibition of new synthesized thiophene Schiff base on mild steel X52 in HCl and H2SO4 solutions, Corros. Sci. 79 (2014) 50–58, https://doi.org/10.1016/j.corsci.2013.10.025.
[80] B.D. Mert, A.O. Yüce, G. Kardaş, B. Yazıcı, Inhibition effect of 2-amino-4-methylpyridine on mild steel corrosion: Experimental and theoretical investigation, Corros. Sci. 85 (2014) 287–295, https://doi.org/10.1016/j.corsci.2014.04.032.
[81] E. Bayol, T. Gürten, A.A. Gürten, M. Erbil, Interactions of some Schiff base compounds with mild steel surface in hydrochloric acid solution, Mater. Chem. Phys. 112 (2008) 624–630, https://doi.org/10.1016/j.matchemphys.2008.06.012.
[82] A.A. Farag, T.A. Ali, The enhancing of 2-pyrazinecarboxamide inhibition effect on the acid corrosion of carbon steel in presence of iodide ions, J. Ind. Eng. Chem. 21 (2015) 627–634, https://doi.org/10.1016/j.jiec.2014.03.030.
[83] H.H. Zhang, Y. Chen, Experimental and theoretical studies of benzaldehyde thiosemicarbazone derivatives as corrosion inhibitors for mild steel in acid media, J. Mol. Struct. 1177 (2019) 90–100, https://doi.org/10.1016/j.molstruc.2018.09.048.
[84] M.A. Migahed, A.A. Farag, S.M. Elsaed, R. Kamal, H.A. El-Bary, Corrosion Inhibition of Steel Pipelines in Oil Well Formation Water By a New Family of Nonionic Surfactants, Chem. Eng. Commun. 199 (2012) 1335–1356, https://doi.org/10.1080/00986445.2012.662922.
[85] B. Xu, W. Yang, Y. Liu, X. Yin, W. Gong, Y. Chen, Experimental and theoretical evaluation of two pyridinecarboxaldehyde thiosemicarbazone compounds as corrosion inhibitors for mild steel in hydrochloric acid solution, Corros. Sci. 78 (2014) 260–268, https://doi.org/10.1016/j.corsci.2013.10.007.
[86] H. Hamani, T. Douadi, M. Al-Noaimi, S. Issaadi, D. Daoud, S. Chafaa, Electrochemical and quantum chemical studies of some azomethine compounds as corrosion inhibitors for mild steel in 1M hydrochloric acid, Corros. Sci. 88 (2014) 234–245, https://doi.org/10.1016/j.corsci.2014.07.044.
[87] E.E. Elemike, D.C. Onwudiwe, H.U. Nwankwo, E.C. Hosten, Synthesis, crystal structure, electrochemical and anti-corrosion studies of Schiff base derived

from o-toluidine and o-chlorobenzaldehyde, J. Mol. Struct. 1136 (2017) 253–262, https://doi.org/10.1016/j.molstruc.2017.01.085.
[88] N.D. Nam, Q.V. Bui, M. Mathesh, M.Y.J. Tan, M. Forsyth, A study of 4-carboxyphenylboronic acid as a corrosion inhibitor for steel in carbon dioxide containing environments, Corros. Sci. 76 (2013) 257–266, https://doi.org/10.1016/j.corsci.2013.06.048.
[89] A. Kosari, M.H. Moayed, A. Davoodi, R. Parvizi, M. Momeni, H. Eshghi, H. Moradi, Electrochemical and quantum chemical assessment of two organic compounds from pyridine derivatives as corrosion inhibitors for mild steel in HCl solution under stagnant condition and hydrodynamic flow, Corros. Sci. 78 (2014) 138–150, https://doi.org/10.1016/j.corsci.2013.09.009.
[90] L. Zeng, G.A. Zhang, X.P. Guo, C.W. Chai, Inhibition effect of thioureidoimidazoline inhibitor for the flow accelerated corrosion of an elbow, Corros. Sci. 90 (2015) 202–215, https://doi.org/10.1016/j.corsci.2014.10.011.
[91] V. Sastri, Corrosion Inhibitors: Principles and Applications, John Wiley and Sons, New York, 1998.
[92] M. Scendo, Corrosion inhibition of copper by purine or adenine in sulphate solutions, Corros. Sci. 49 (2007) 3953–3968, https://doi.org/10.1016/j.corsci.2007.03.037.
[93] N. Kıcır, G. Tansuğ, M. Erbil, T. Tüken, Investigation of ammonium (2,4-dimethylphenyl)-dithiocarbamate as a new, effective corrosion inhibitor for mild steel, Corros. Sci. 105 (2016) 88–99, https://doi.org/10.1016/j.corsci.2016.01.006.
[94] A.K. Singh, M.A. Quraishi, Investigation of the effect of disulfiram on corrosion of mild steel in hydrochloric acid solution, Corros. Sci. 53 (2011) 1288–1297, https://doi.org/10.1016/j.corsci.2011.01.002.
[95] L.O. Olasunkanmi, M.F. Sebona, E.E. Ebenso, Influence of 6-phenyl-3(2H)-pyridazinone and 3-chloro-6-phenylpyrazine on mild steel corrosion in 0.5 M HCl medium: Experimental and theoretical studies, J. Mol. Struct. 1149 (2017) 549–559, https://doi.org/10.1016/j.molstruc.2017.08.018.
[96] M. Tourabi, K. Nohair, M. Traisnel, C. Jama, F. Bentiss, Electrochemical and XPS studies of the corrosion inhibition of carbon steel in hydrochloric acid pickling solutions by 3,5-bis(2-thienylmethyl)-4-amino-1,2,4-triazole, Corros. Sci. 75 (2013) 123–133, https://doi.org/10.1016/j.corsci.2013.05.023.
[97] L.S.M.G. Hosseini, H. Khalilpur, S. Ershad, Protection of mild steel corrosion with new thia-derivative Salens in 0.5 M H2SO4 solution, J. Appl. Electrochem. 40 (2010) 215–223.
[98] A. Döner, E.A. Şahin, G. Kardaş, O. Serindağ, Investigation of corrosion inhibition effect of 3-[(2-hydroxy-benzylidene)-amino]-2-thioxo-thiazolidin-4-one on corrosion of mild steel in the acidic medium, Corros. Sci. 66 (2013) 278–284, https://doi.org/10.1016/j.corsci.2012.09.030.
[99] I. Ahamad, R. Prasad, M.A. Quraishi, Inhibition of mild steel corrosion in acid solution by Pheniramine drug: Experimental and theoretical study, Corros. Sci. 52 (2010) 3033–3041, https://doi.org/10.1016/j.corsci.2010.05.022.
[100] R. Solmaz, Investigation of adsorption and corrosion inhibition of mild steel in hydrochloric acid solution by 5-(4-Dimethylaminobenzylidene)rhodanine, Corros. Sci. 79 (2014) 169–176, https://doi.org/10.1016/j.corsci.2013.11.001.
[101] M.J. Bahrami, S.M.A. Hosseini, P. Pilvar, Experimental and theoretical investigation of organic compounds as inhibitors for mild steel corrosion in sulfuric acid medium, Corros. Sci. 52 (2010) 2793–2803, https://doi.org/10.1016/j.corsci.2010.04.024.
[102] A.S. Ismail, A.A. Farag, Experimental, theoretical and simulation studies of extracted crab waste protein as a green polymer inhibitor for carbon steel corrosion in 2 M H 3 PO 4, Surf. Interfaces 19 (2020) 100483, https://doi.org/10.1016/j.surfin.2020.100483.
[103] E. Kuş, F. Mansfeld, An evaluation of the electrochemical frequency modulation (EFM) technique, Corros. Sci. 48 (2006) 965–979, https://doi.org/10.1016/j.corsci.2005.02.023.
[104] Y. Sasikumar, A.S. Adekunle, L.O. Olasunkanmi, I. Bahadur, R. Baskar, M.M. Kabanda, I.B. Obot, E.E. Ebenso, Experimental, quantum chemical and Monte Carlo simulation studies on the corrosion inhibition of some alkyl imidazolium ionic liquids containing tetrafluoroborate anion on mild steel in acidic medium, J. Mol. Liq. 211 (2015) 105–118, https://doi.org/10.1016/j.molliq.2015.06.052.
[105] L. Herrag, B. Hammouti, S. Elkadiri, A. Aouniti, C. Jama, H. Vezin, F. Bentiss, Adsorption properties and inhibition of mild steel corrosion in hydrochloric solution by some newly synthesized diamine derivatives: Experimental and theoretical investigations, Corros. Sci. 52 (2010) 3042–3051, https://doi.org/10.1016/j.corsci.2010.05.024.
[106] H. Elmsellem, M.H. Youssouf, A. Aouniti, T. Ben Hadda, A. Chetouani, B. Hammouti, Adsorption and inhibition effect of curcumin on mild steel corrosion in hydrochloric acid, Russ. J. Appl. Chem. 87 (2014) 744–753, https://doi.org/10.1134/s1070427214060147.
[107] M.A. Deyab, Sulfonium-based ionic liquid as an anticorrosive agent for thermal desalination units, J. Mol. Liq. 296 (2019) 111742.
[108] H. Allal, Y. Belhocine, E. Zouaoui, Computational study of some thiophene derivatives as aluminium corrosion inhibitors, J. Mol. Liq. 265 (2018) 668–678.
[109] B. Tüzün, C. Kaya, Investigation of DNA–RNA molecules for the efficiency and activity of corrosion inhibition by DFT and molecular docking, J. Bio-and Tribo-Corrosion. 4 (2018) 69.
[110] S. Kaya, P. Banerjee, S.K. Saha, B. Tüzün, C. Kaya, Theoretical evaluation of some benzotriazole and phospono derivatives as aluminum corrosion inhibitors: DFT and molecular dynamics simulation approaches, RSC Adv. 6 (2016) 74550–74559.
[111] P.H. Scudder, Electron Flow in Organic Chemistry: A Decision-Based Guide to Organic Mechanisms, John Wiley & Sons, 2013.
[112] N.L. Allinger, Molecular Structure: Understanding Steric and Electronic Effects from Molecular Mechanics, John Wiley & Sons, 2010.
[113] D.S. Chauhan, V. Srivastava, P.G. Joshi, M.A. Quraishi, PEG cross-linked Chitosan: a biomacromolecule as corrosion inhibitor for sugar industry, Int. J. Ind. Chem. 9 (2018) 363–377, https://doi.org/10.1007/s40090-018-0165-0.
[114] Y. Qiang, S. Zhang, L. Guo, S. Xu, L. Feng, I.B. Obot, S. Chen, Sodium dodecyl benzene sulfonate as a sustainable inhibitor for zinc corrosion in 26% NH 4 Cl solution, J. Clean. Prod. 152 (2017) 17–25, https://doi.org/10.1016/j.jclepro.2017.03.104.
[115] F. Weinhold, C.R. Landis, E.D. Glendening, What is NBO analysis and how is it useful?, Int. Rev. Phys. Chem. 35 (2016) 399–440, https://doi.org/10.1080/0144235x.2016.1192262.
[116] G. Frenking, N. Fröhlich, The Nature of the Bonding in Transition-Metal Compounds, Chem. Rev. 100 (2000) 717–774, https://doi.org/10.1021/cr980401l.
[117] A. Hoffmann, F. Ulrich, S. Herres-Pawlisa, Syntheses and characterisation of tris(3-(pyridin-2-yl)-1H-pyrazol-1-yl)methane and its bis(μ-hydroxo) dicobalt(II) complex, Arkivoc. 2012 (2012) 343, https://doi.org/10.3998/ark.5550190.0013.324.
[118] M. Olivucci, A. Sinicropi, Computational Photochemistry, Theor. Comput. Chem. (2005) 1–33, https://doi.org/10.1016/s1380-7323(05)80018-4.
[119] D. Chatfield, J. Christopher, Cramer: Essentials of Computational Chemistry: Theories and Models, Theor. Chem. Accounts Theory, Comput. Model. (Theoretica Chim. Acta) 108 (2002) 367–368, https://doi.org/10.1007/s00214-002-0380-8.
[120] L.H. Madkour, S. Kaya, I.B. Obot, Computational, Monte Carlo simulation and experimental studies of some arylazotriazoles (AATR) and their copper complexes in corrosion inhibition process, J. Mol. Liq. 260 (2018) 351–374, https://doi.org/10.1016/j.molliq.2018.01.055.
[121] R. Hsissou, S. Abbout, A. Berisha, M. Berradi, M. Assouag, N. Hajjaji, A. Elharfi, Experimental, DFT and molecular dynamics simulation on the inhibition performance of the DGDCBA epoxy polymer against the corrosion of the E24 carbon steel in 1.0 M HCl solution, J. Mol. Struct. 1182 (2019) 340–351, https://doi.org/10.1016/j.molstruc.2018.12.030.
[122] A.S. Fouda, G.Y. Elewady, K. Shalabi, H.K. Abd El-Aziz, Alcamines as corrosion inhibitors for reinforced steel and their effect on cement based materials and mortar performance, RSC Adv. 5 (2015) 36957–36968, https://doi.org/10.1039/c5ra00717h.
[123] A. Mottais, M. Berchel, Y. Sibiril, V. Laurent, D. Gill, S. Hyde, P.-A. Jaffrès, T. Montier, T. Le Gall, Antibacterial effect and DNA delivery using a combination of an arsonium-containing lipophosphoramide with an N-heterocyclic carbene-silver complex – Potential benefits for cystic fibrosis lung gene therapy, Int. J. Pharm. 536 (2018) 29–41, https://doi.org/10.1016/j.ijpharm.2017.11.022.
[124] T.J. Silhavy, D. Kahne, S. Walker, The bacterial cell envelope, Cold Spring Harb. Perspect. Biol. 2 (2010) a000414.
[125] F. Karabudak, R. Yeşildal, E.E. Şüküroğlu, S. Şüküroğlu, H. Zamanlou, N. Dikbaş, F. Bayındır, S. Şen, Y. Totik, An Investigation of Corrosion Resistance and Antibacterial Sensitivity Properties of Nano-Ag-Doped $$\hbox{{TiO}_{2}$$TiO2Coating and $$\hbox{{TiO}_{2}$$TiO2Coating Grown on NiTi Alloy with the Micro-Arc Oxidation Process, Arab. J. Sci. Eng. 42 (2017) 2329–2339, https://doi.org/10.1007/s13369-017-2463-9.
[126] K.M. Takroni, H.A. El-Ghamry, A. Fawzy, Evaluation of the Catalytic Activities of Some Synthesized Divalent and Trivalent Metal Complexes and Their Inhibition Efficiencies for the Corrosion of Mild Steel in Sulfuric Acid Medium, J. Inorg. Organomet. Polym Mater. 29 (2019) 1927–1940.
[127] G.H. Sayed, M.E. Azab, K.E. Anwer, M.A. Raouf, N.A. Negm, Pyrazole, pyrazolone and enaminonitrile pyrazole derivatives: Synthesis, characterization and potential in corrosion inhibition and antimicrobial applications, J. Mol. Liq. 252 (2018) 329–338.
[128] A.A. Migahed, M.A. Negm, N.A. Shaban, M.M. Ali, T.A. Fadda, Synthesis, characterization, surface and biological activity of diquaternary cationic surfactants containing ester linkage, J. Surfactants Deterg. 19 (2016) 119–128.
[129] Y. Konno, A.A. Farag, E. Tsuji, Y. Aoki, H. Habazaki, Formation of porous anodic films on carbon steels and their application to corrosion protection composite coatings formed with polypyrrole, J. Electrochem. Soc. (2016), https://doi.org/10.1149/2.1451607jes.
[130] M. Cui, S. Ren, Q. Xue, H. Zhao, L. Wang, Carbon dots as new eco-friendly and effective corrosion inhibitor, J. Alloy. Compd. 726 (2017) 680–692, https://doi.org/10.1016/j.jallcom.2017.08.027.
[131] A.A. Farag, Oil-in-water emulsion of a heterocyclic adduct as a novel inhibitor of API X52 steel corrosion in acidic solution, Corros. Rev. 36 (2018) 575–588, https://doi.org/10.1515/corrrev-2018-0002.
[132] A.A. Farag, M.A. Migahed, E.A. Badr, Thiazole Ionic Liquid as Corrosion Inhibitor of Steel in 1 M HCl Solution: Gravimetrical, Electrochemical, and Theoretical Studies, J. Bio- Tribo-Corrosion. 5 (2019) 53, https://doi.org/10.1007/s40735-019-0246-4.
[133] A.A. Farag, E.A. Badr, Original article Non-ionic surfactant loaded on gel capsules to protect downhole tubes from produced water in acidizing oil wells, Corros. Rev. 38 (2020) 151–164, https://doi.org/10.1515/corrrev-2019-0030.
[134] C. Verma, L.O. Olasunkanmi, I. Bahadur, H. Lgaz, M.A. Quraishi, J. Haque, E.-S. M. Sherif, E.E. Ebenso, Experimental, density functional theory and molecular

dynamics supported adsorption behavior of environmental benign imidazolium based ionic liquids on mild steel surface in acidic medium, J. Mol. Liq. 273 (2019) 1–15, https://doi.org/10.1016/j.molliq.2018.09.139.

[135] A. Dehghani, G. Bahlakeh, B. Ramezanzadeh, M. Ramezanzadeh, Potential of Borage flower aqueous extract as an environmentally sustainable corrosion inhibitor for acid corrosion of mild steel: Electrochemical and theoretical studies, J. Mol. Liq. 277 (2019) 895–911, https://doi.org/10.1016/j.molliq.2019.01.008.

[136] H.F. Xianghong Li, Shuduan Deng, Triazolyl blue tetrazolium bromide as a novel corrosion inhibitor for steel in HCl and H2SO4 solutions, Corros. Sci. 53 (2011) 302–309.

[137] J. Aljourani, K. Raeissi, M.A. Golozar, Benzimidazole and its derivatives as corrosion inhibitors for mild steel in 1M HCl solution, Corros. Sci. 51 (2009) 1836–1843, https://doi.org/10.1016/j.corsci.2009.05.011.

[138] M. Murmu, S.K. Saha, N.C. Murmu, P. Banerjee, Effect of stereochemical conformation into the corrosion inhibitive behaviour of double azomethine based Schiff bases on mild steel surface in 1 mol L−1 HCl medium: An experimental, density functional theory and molecular dynamics simulation study, Corros. Sci. 146 (2019) 134–151, https://doi.org/10.1016/j.corsci.2018.10.002.

[139] Q.B. Zhang, Y.X. Hua, Corrosion inhibition of mild steel by alkylimidazolium ionic liquids in hydrochloric acid, Electrochim. Acta 54 (2009) 1881–1887, https://doi.org/10.1016/j.electacta.2008.10.025.

[140] M.A.M. Ahmed, A. Farag, Amr S. Ismail, 2020-Bio&Tribo-corr. Squid By-product Gelatin Polymer as an Eco-friendly Corrosion Inhibitor.pdf, J. Bio-Tribo-Corrosion. 6 (2020) 16, https://doi.org/10.1007/s40735-019-0310-0.

[141] N.S. Patel, P. Beranek, M. Nebyla, M. Přibyl, D. Šnita, Inhibitive effects by some benzothiazole derivatives on mild steel corrosion in 1 N HCl, Int. J. Electrochem. Sci. 9 (2014) 3951–3960.

[142] H. Jafari, K. Akbarzade, I. Danaee, Corrosion inhibition of carbon steel immersed in a 1 M HCl solution using benzothiazole derivatives, Arab. J. Chem. 12 (2019) 1387–1394, https://doi.org/10.1016/j.arabjc.2014.11.018.

[143] K. Parameswari, S. Chitra, A. Selvaraj, S. Brindha, M. Menaga, Investigation of benzothiazole derivatives as corrosion inhibitors for mild steel, Port. Electrochim. Acta 30 (2012) 89–98, https://doi.org/10.4152/pea.201202089.

[144] Z. Salarvanda, M. Amirnasr, M. Talebian, K. Raeissi, S. Meghdadi, Enhanced corrosion resistance of mild steel in 1 M HCl solution by trace amount of 2-phenyl-benzothiazole derivatives: experimental, quantum chemical calculations and mo-lecular dynamics (MD) simulation studies, Corros. Sci. 114 (2017) 133–145, https://doi.org/10.1016/j.corsci.2016.11.002.

[145] Z. Hu, Y. Meng, X. Ma, H. Zhu, J. Li, C. Li, D. Cao, Experimental and theoretical studies corrosion of benzothiazole derivatives as inhibitors for carbon steel in 1M HCl, Corros. Sci. 112 (2016) 563–575, https://doi.org/10.1016/j.corsci.2016.08.012.

[146] S.K. Dutta, P. Saha, D. Banerjee, Sukul, Correlating electronic structure with corro-sion inhibition potentiality of some bis-benzimidazole derivatives for mild steel in hydrochloric acid: combined experimental and theoretical studies, Corros. Sci. 98 (2015) 541–550, https://doi.org/10.1016/j.corsci.2015.05.065.